

Facility for spectral irradiance and radiance responsivity calibrations using uniform sources

Steven W. Brown, George P. Eppeldauer, and Keith R. Lykke

Detectors have historically been calibrated for spectral power responsivity at the National Institute of Standards and Technology by using a lamp–monochromator system to tune the wavelength of the excitation source. Silicon detectors can be calibrated in the visible spectral region with combined standard uncertainties at the 0.1% level. However, uncertainties increase dramatically when measuring an instrument's spectral irradiance or radiance responsivity. We describe what we believe to be a new laser-based facility for spectral irradiance and radiance responsivity calibrations using uniform sources (SIRCUS) that was developed to calibrate instruments directly in irradiance or radiance mode with uncertainties approaching or exceeding those available for spectral power responsivity calibrations. In SIRCUS, the emission from high-power, tunable lasers is introduced into an integrating sphere using optical fibers, producing uniform, quasi-Lambertian, high-radiant-flux sources. Reference standard irradiance detectors, calibrated directly against national primary standards for spectral power responsivity and aperture area measurement, are used to determine the irradiance at a reference plane. Knowing the measurement geometry, the source radiance can be readily determined as well. The radiometric properties of the SIRCUS source coupled with state-of-the-art transfer standard radiometers whose responsivities are directly traceable to primary national radiometric scales result in typical combined standard uncertainties in irradiance and radiance responsivity calibrations of less than 0.1%. The details of the facility and its effect on primary national radiometric scales are discussed.

OCIS codes: 120.0120, 120.5630, 120.3930.

1. Introduction

Detectors are calibrated for spectral power responsivity over the spectral range from 350 to 1000 nm at the National Institute of Standards and Technology (NIST) on the spectral comparator facility¹ (SCF) by using a lamp–monochromator system to tune the wavelength of the excitation source and silicon working standard detectors with responsivities directly traceable to the NIST high-accuracy cryogenic radiometer (HACR), the primary U.S. national radiometric standard for optical power measurement.^{2,3} Silicon detectors can be calibrated for optical power responsivity in the visible spectral region on the SCF with combined expanded uncertainties ($k = 2$) at the 0.2% level. However, quantities of interest are often the amount of light falling on a surface (irradiance) or the amount of light emitted from a source (radiance). In many cases, spectral information is required as

well. Consequently, the calibration of filter-based irradiance and radiance meters is frequently needed.

Because of the low flux in the lamp–monochromator system, instruments cannot be directly calibrated for irradiance or radiance responsivity on the SCF, and more complicated approaches must be taken that often increase the expanded uncertainty ($k = 2$) in the measurements to the 0.5% level or greater.⁴ In addition, the low flux associated with lamp–monochromator excitation sources ($\sim 1 \mu\text{W}$) limits the effective dynamic range of the system. The out-of-band response of filter radiometers can be measured only to approximately 0.001% of the peak response while a dynamic range greater than 10^6 can be required for high-accuracy applications. In more advanced applications, spatially nonuniform (e.g., infrared or ultraviolet) irradiance meters cannot be calibrated accurately by using the traditional power measurement mode on the SCF and detector-array-based imaging systems require tests in uniform, monochromatic fields.

With the development of tunable dye lasers in 1970,^{5,6} high-power, monochromatic, tunable sources became available for scientific use. Replacing the lamp–monochromator source with a tunable laser

The authors are with the National Institute of Standards and Technology, Gaithersburg, Maryland 20899. S. Brown's e-mail address is steven.brown@nist.gov.

Received 14 February 2006; accepted 27 April 2006; posted 7 July 2006 (Doc. ID 68064).

source has a number of advantages for radiometric applications, in particular the high-power, very narrow spectral bandwidth, and the extremely low wavelength uncertainty of the laser-based source. Schaefer and Eckerle⁷ developed the first laser-based radiometric facility at NIST in 1984. In 1986, independent irradiance scales maintained by NIST based on blackbody or synchrotron radiation were compared with scales established on the laser calibration facility based on silicon photodiode physics traceable to cryogenic radiometry.⁸ In 1990, absolute spectral radiometric measurements of the melting and freezing points of a gold blackbody were made at NIST using the laser-based facility.⁹ The radiometric temperature was in agreement with the gold-point value established in the International Temperature Scale of 1990 (ITS-90). In the same time frame, a laser-based radiometric calibration facility was established at the National Physical Laboratory (NPL) in the United Kingdom, and the radiometric freezing and melting temperatures of gold, silver, and aluminum blackbodies were determined with a radiometric uncertainty of 0.04%.¹⁰ The results were compared with thermodynamic temperatures established by using constant-volume gas thermometry. Subsequently, several primary national radiometric standards laboratories have developed or are developing laser-based calibration facilities, including the NPL in the UK,¹¹ the Helsinki University of Technology (HUT) in Finland,¹² and the Physikalisch-Technische Bundesanstalt (PTB) in Germany,¹³ as well as at NIST. In this work, a new laser-based facility developed at NIST for spectral irradiance and radiance responsivity calibrations using uniform sources (SIRCUS) is described.

This facility expands on previous work through the integration of cw, continuously tunable lasers that cover wide ranges of the spectrum as well as with the development of high-performance transfer standard detectors. The expanded continuous spectral coverage has been made possible by recent and continued advances in laser technology. By exploiting the developments in laser and detector technologies in SIRCUS and calibrating filter radiometers that are used in radiance temperature (pyrometers) and photometry (photometers), the uncertainty of the two Systeme Internationale (SI) units maintained by the NIST Optical Technology Division, the kelvin and the candela, can be reduced.

In Section 2 we describe the principal components of the facility and give a representative uncertainty budget for an instrument calibration. In Section 3 we compare the SCF with SIRCUS. In Section 4 we discuss the effect on NIST scales and facilities. In Section 5, we give examples of calibrations that illustrate the flexibility of the new facility.

2. Description of Spectral Irradiance and Radiance Responsivity Calibrations Using Uniform Sources

In the SIRCUS facility, emission from high-power, tunable lasers is introduced into an integrating sphere producing uniform, quasi-Lambertian, highly radiant

flux sources. Reference standard irradiance detectors, calibrated directly against national primary standards for spectral power responsivity, are used to determine the irradiance at a reference plane. Knowing the measurement geometry, the source radiance can be readily determined as well. Instruments are calibrated directly in irradiance or radiance mode with uncertainties approaching or exceeding those available for spectral power responsivity calibrations.

There are three components to the SIRCUS facility: an ultraviolet, visible, and near-infrared (UV-Vis-NIR) SIRCUS; an infrared (IR) SIRCUS; and a high-accuracy electrical substitution cryogenic radiometer system called the primary optical watt radiometer (POWR).¹⁴ POWR is a primary standard facility for the measurement of optical power. The UV-Vis-NIR facility currently operates over the spectral region from 210 to 960 nm; extensions to the short-wave IR, out to 2.5 μm , are planned. The IR SIRCUS facility has a spectral coverage from 700 to 5.3 μm using tunable optical parametric oscillator (OPO) systems and coverage to 11 μm using discrete laser sources. Lasers from both SIRCUS facilities can be introduced into the POWR radiometer for detector responsivity measurements. Typically, reference instruments used on SIRCUS are calibrated against POWR. Occasionally, a second, working-standard absolute cryogenic radiometer (ACR) is used.¹⁵ This system is smaller and easier to operate than POWR. It is located on a portable table and can be readily moved between facilities. Intercomparisons using transfer standard detectors establish the equivalence between the two cryogenic radiometers.

The spectral coverage available with the tunable lasers ultimately defines the spectral range of the SIRCUS facility while the quality of the reference standard detectors and their radiometric uncertainties ultimately determine the uncertainty achievable on SIRCUS. In this work we focus on the UV-Vis-NIR facility and limit the discussion to the spectral range from 210 to 960 nm where silicon reference detectors are available. A general description of the SIRCUS facility is given in Subsection 2.A. Sources and reference detectors are discussed in Subsections 2.B and 2.C. Subsection 2.D outlines the calibration method. The uncertainties achievable for radiance and irradiance responsivity calibrations are discussed in Subsection 2.E.

It should be noted that our identification of commercial equipment is for information purposes only. It does not imply recommendation or endorsement by the National Institute of Standards and Technology, nor does it imply that the equipment identified is necessarily the best available for the purpose.

A. Setup

The SIRCUS facility is shown schematically in Fig. 1. The output of a high-power, tunable laser is first directed through an intensity stabilizer that controls the relative optical power in the beam to within 0.1% of the set point. A portion of the laser beam is sent into a traveling Michelson interferometer that mea-

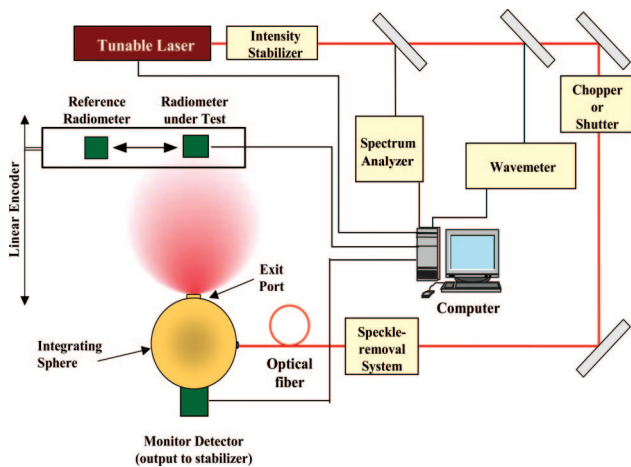


Fig. 1. (Color online) Schematic diagram of the SIRCUS facility.

ures the wavelength of the radiation to within 0.001 nm. A beam splitter sends another portion of the laser beam into a Fabry–Perot interferometer to measure the bandwidth and mode stability of the laser. The laser radiation is typically introduced into an integrating sphere, often using an optical fiber. Different size spheres are used depending on the application. Occasionally, a collimator coupled to the sphere is used as a calibration source. Speckle in the image from the source, originating from interference due to the coherent nature of the laser radiation, is effectively removed either by rastering the beam inside the sphere with a galvanometer-driven mirror⁹ or by placing a short length of optical fiber in an ultrasonic bath.^{11,16} Note that the speckle is still present but is altered on a much shorter time constant than the observing radiometers, effectively averaging out the distribution. A monitor photodiode is located on the sphere to correct for any radiant flux changes in the sphere output between measurements with the reference instrument and the device under test. The sources and detectors are located inside a light-tight box (1.4 m wide, 1.2 m tall, 3.2 m long) that has been covered on the inside with Ultrapol, a material with excellent light-absorbing properties: The measured reflectance is of the order of 0.1%–0.3% from 300 nm to 2.5 μm . Two baffles are typically installed between the source and the detectors to minimize the effects of stray radiation on the measurement.

The calibrations are performed by direct substitution against primary standard reference irradiance meters (see Subsection 2.C). For both irradiance and radiance responsivity calibrations, the distance between the source aperture and the defining aperture on the reference standard detector is required. An electronic ruler with a resolution of 5 μm measures the distance between the source and the detectors.

B. Sources

In this subsection we go into detail on the laser systems as well as the different calibration sources,

namely, the integrating spheres and collimators used on SIRCUS.

1. Lasers

A number of different lasers are used to cover the spectral range from about 210 to 960 nm (see Fig. 2). Continuous tunability is provided by dye lasers and Ti:sapphire lasers that are pumped by either an argon-ion laser (25 W, all lines visible; 7 W, all lines UV) or a frequency-doubled Nd:vanadate laser (10 W, 532 nm). A number of discrete wavelengths are provided by the pump lasers themselves.

Dye laser use has declined in recent years because of the development of the solid-state Ti:sapphire laser, but the dye laser is still the easiest method for producing high-power, tunable, cw light in the visible.^{17,18} Dye lasers at SIRCUS cover the spectral region from 415 to 700 nm; the dyes used include Stilbene 3 (415–475 nm), Coumarin 480 (470–520 nm), Coumarin 521 (505–565 nm),¹⁹ Rhodamine 6G (R6G; 550–620 nm), and DCM (610–700 nm). A separate laser is used for each dye so that the full tuning range can be rapidly covered, and no dye change or optical reconfiguration is required. The longer-wavelength dye lasers, with DCM and R6G dyes, are ring lasers. They are located on a table separate from the other three dye lasers and are pumped by the 532 nm output from a frequency-doubled Nd:vanadate laser. The Coumarin 521, Coumarin 480, and Stilbene 3 lasers are pumped with the output of an argon-ion laser. Separate optical fibers, located on each laser table, couple the radiation from the lasers into the integrating spheres.

Ti:sapphire lasers cover the spectral range from 680 to 1050 nm.²⁰ A frequency doubling of Ti:sapphire lasers enables us to tune from 350 to 500 nm. Two different types of frequency doubling are available: The first approach uses an external power buildup cavity that requires a frequency-stabilized, single-mode pump laser.²¹ The second is a home-built intracavity-doubled Ti:sapphire laser that requires no frequency stabilization. This system uses a simple

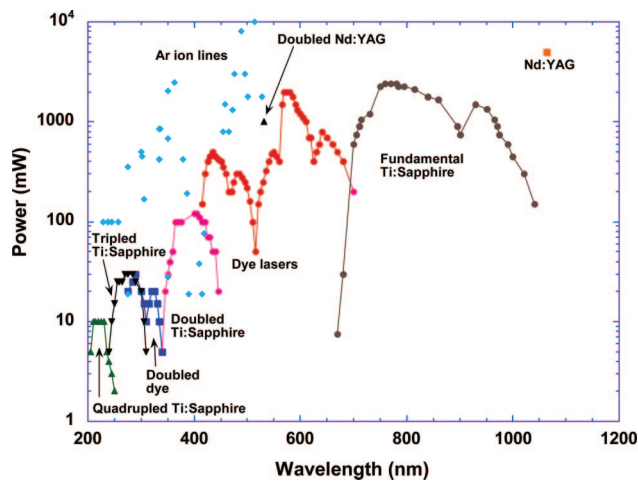


Fig. 2. (Color online) Lasers, output power, and spectral coverage of UV–Vis–IR SIRCUS.

z-cavity Ti:sapphire laser. When doubling is required, the output coupler is removed and two mirrors are used in its place: a fold mirror (with a 5 cm focal length) and a flat mirror. The doubling crystal, typically lithium barium oxide (LBO), is located near the focus of the curved mirror.²² One of the attractive features of the intracavity-doubling design is that the system lases without the doubling crystal in place—ensuring the proper cavity alignment prior to installation of the doubling crystal. It is also less sensitive to acoustic noise and small frequency fluctuations in the laser than the external-cavity system.

Over 300 mW of optical power is available from the dye lasers and the Ti:sapphire laser (with optical powers of 1 W or greater over much of the spectral range). The power available from the cw, frequency-doubled radiation is typically in the range from 100 to 200 mW. A variety of standing-wave and ring lasers are currently used on SIRCUS. With the exception of the external buildup cavity approach to frequency-doubled light, simple, inexpensive standing-wave dye lasers and Ti:sapphire lasers equipped with an intracavity, uncoated etalon to ensure narrowband operation are sufficient for all foreseeable radiometric applications.

Quasi-cw, mode-locked laser systems have been shown in the past to be equivalent to cw systems for radiometric calibrations of silicon radiometers, with no additional uncertainties in the calibration arising from the quasi-cw nature of the radiation.^{23,24} A commercial mode-locked system was recently installed in the facility. The system includes an OPO system for generation of visible and infrared light, and a frequency doubler, tripler, and quadrupler system for generation of visible and UV radiation. These nonlinear optical systems take advantage of the pulsed nature of the radiation: It is significantly easier to generate sum and difference frequency radiation using a mode-locked laser rather than a true cw laser because of the high peak power of the mode-locked source. This system generates almost continuously tunable radiation from 210 to 3 μm . One useful feature of the quasi-cw system is that the bandwidth of the radiation is considerably broader than radiation from the cw systems. This may help to alleviate the measurement problems associated with interference fringes (discussed in Section 6).

Computer-controlled actuators rotate the angle of the birefringent tuner in the dye and Ti:sapphire lasers. The minimum step size is determined by the free spectral range of the etalon in the lasers. For a 1 mm thick etalon, the thickness of the etalons used on SIRCUS, the minimum wavelength step using the birefringent tuner is 0.16 nm at 600 nm. For finer spectral resolution, the etalon angle is changed as well. Controlling both the birefringent tuner and the etalon angle, wavelength steps of 0.01 nm or less can be readily achieved.

2. Integrating Spheres

Different integrating spheres are used, depending on the radiometric calibration. Small-diameter integrat-

ing spheres—with diameters ranging from 2.54 to 5.08 cm—equipped with precision apertures with diameters ranging from 3 to 8 mm are typically used for irradiance responsivity calibrations. Note that the areas of the exit apertures are normally measured at the NIST facility for aperture area measurement.²⁵ Larger-diameter spheres—30 cm in diameter—with 5 to 10 cm diameter exit ports are used for radiance measurements. The spheres are made of a sintered polytetrafluoroethylene-based (PTFE-based) coating that has high diffuse reflectance from approximately 250 nm to 2.5 μm .²⁶ Typical irradiance levels at 1 m using a 2.54 cm diameter integrating sphere with a 5 mm diameter aperture range from approximately 1 to 10 $\mu\text{W}/\text{cm}^2$. Radiance levels between 1 and 5 $\text{mW}/\text{cm}^2/\text{sr}$ are standard for a 30 cm diameter sphere with a 7.5 cm diameter output port. A monitor detector is mounted on the sphere wall to monitor and correct for fluctuations in the source radiant flux during a calibration. The irradiance is uniform to within 0.1% over several centimeters at a 1 m separation from the integrating sphere. Similarly, the radiance from the integrating sphere is uniform to within 0.1% over the central 90% of the exit aperture.

3. Collimator Sources

In earlier work at the NPL, collimated sources made from spheres with lenses were used in the calibration of a number of filter radiometers and transmission of lenses.¹¹ In SIRCUS, off-axis parabolic mirrors are used to prepare the quasi-collimated source. Mirrors have the advantage over lenses of achromaticity from the UV to the IR. In addition to the collimators in SIRCUS, both on- and off-axis collimator sources have been developed in collaboration with NASA²⁷ and the U.S. Geological Survey²⁸ (USGS) for the characterization and calibration of large-aperture-area telescopes. Nonuniformities of 1% or less are achieved over a 5 cm diameter area with an irradiance up to 2 orders of magnitude greater than with the integrating sphere alone.

C. Detectors

The uncertainty in the spectral irradiance responsivity of reference standard detectors is the largest component in the SIRCUS calibration uncertainty budget. Ultimately, the quality and characteristics of the reference standard detectors determine the uncertainty achievable on SIRCUS. Silicon tunnel-trap detectors, configured to operate in both radiant power and irradiance measurement modes, are the highest-level reference standards used in the SIRCUS facility. They cover the spectral range from 300 to 960 nm. Reflectance traps with specially designed Si detectors that are stable under UV exposure are used for calibrations in the 210 to 350 nm spectral region.

1. Reference Standard Silicon Tunnel-Trap Detector

Trap detectors consist of multiple silicon photodiodes oriented such that the incident radiation reflected from one detector impinges on a second detector.²⁹ Hamamatsu model S1337 (Ref. 30) photodiodes are

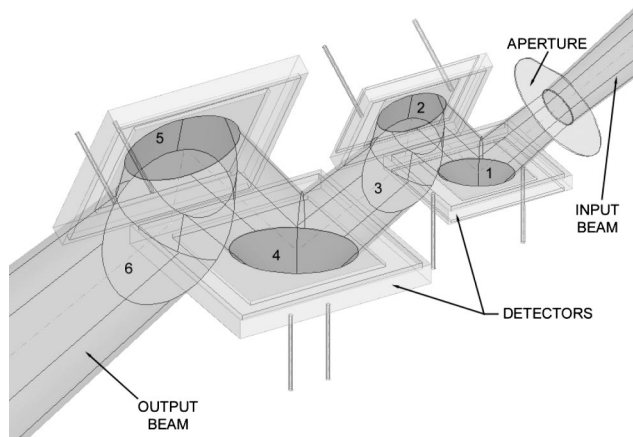


Fig. 3. Beam propagation through the six-element transmission tunnel-trap detector. Detectors 3 and 6 have been removed from the diagram.

typically used in trap detectors to utilize the physical model of internal quantum efficiency (IQE) for spectral responsivity extrapolation and interpolation.³ The IQE is the ratio of the number of collected electrons to the number of photons absorbed by the detector after the front surface reflection loss; the S1337 photodiodes are chosen because of their extremely high IQE (close to 1). A detector's external quantum efficiency (EQE) is equal to the IQE times the term $1 - \text{reflectance}$. In trap detectors, the reflection loss is minimized by having incident reflected radiation impinge on the next photodiode in succession, leading to the absorption of almost all the incident radiation. Measuring the sum of the photocurrents from the photodiodes that make up the trap detector, the EQE can be very close to unity. This type of detector is frequently called a quantum-flat detector.

The schematic of the transmission tunnel-trap detectors used on SIRCUS, with the input aperture included, is shown in Fig. 3.³¹ By choosing different size photodiodes, the aperture area and the field of view (FOV) could be maximized. Two $10 \text{ mm} \times 10 \text{ mm}$ and four $18 \text{ mm} \times 18 \text{ mm}$ silicon photodiodes, equivalent to the Hamamatsu S1337 model photodiodes, were packaged in a triangular-shaped, light-trapping arrangement. The photodiodes were selected for large and equal shunt resistance, an important consideration for the signal current-to-voltage conversion.³¹ The beam propagates in the tunnel-trap detector from the first photodiode (behind the aperture) to the last (sixth) photodiode. Photodiodes 3 and 6 are not shown for better illustration. The small amount of radiation that exits the back of the trap detector can be utilized for alignment or can be measured for detector transmittance measurements in spectral responsivity determination. A conical light trap attached to the trap detector output absorbs the transmitted radiation and minimizes the effect of ambient stray light for low-level optical radiation measurements. The photodiodes in the trap detectors are not temperature controlled. The trap detectors have been characterized for both electri-

cal and optical performance. In Subsection 2.D, the trap detector's response linearity, spatial uniformity, and angular responsivity are discussed along with the spectral power responsivity calibration against a high-accuracy cryogenic radiometer.

2. Monitor Detectors

Silicon detectors mounted on the integrating sphere sources monitor the source radiance and correct for any small changes that occur during a calibration caused by fluctuations in the laser power input into the integrating spheres. To avoid interference fringes in the monitor signal (caused by residual coherence in the output radiation of a sphere source), the window of the silicon monitor detector is removed, or a diffuser is placed between the silicon detector and the integrating sphere. Both the reference standard trap detectors and the monitor detectors operate in dc measurement mode.³²

D. Method of Calibration

A calibration relates the measured quantity from a radiometer, usually current or voltage, to the radiometric quantity being measured, e.g., radiance or irradiance, through the instrument's responsivity. Determination of an instrument's responsivity and an evaluation of the associated uncertainties are required in a calibration. The substitution method is used for calibrations in SIRCUS. NIST reference standard irradiance meters determine the irradiance at a reference plane. From the irradiance at the reference plane, which is usually the plane of the detector aperture, the radiance of a source can be determined by knowing the distance between the detector and source apertures, as well as the area of the source aperture. The instrument being calibrated, or device under test (DUT), is then placed in front of the source and its signal is recorded. The laser is blocked and the dark signal is recorded prior to each measurement. The responsivity (at the excitation wavelength) is the instrument's net output signal (with the dark signal subtracted from the light signal) divided by the radiometric quantity to be measured.

The characterization of an instrument and an understanding and evaluation of all meaningful sources of uncertainty are crucial for a proper calibration. A calibration without an associated uncertainty table is of limited use. The evaluation and expression of uncertainty is generally difficult and time consuming; it is not unusual to have incomplete or inaccurate information in an uncertainty table. Determining how best to express a particular uncertainty component can be confusing. There are a variety of useful references that provide definitions and recommendations for describing and establishing the uncertainties encountered when calibrating a radiometer.³³

A measurement equation is a mathematical expression describing the relationship between the measured source-related radiometric quantity and the instrument responsivity. The simplified measurement equation for an irradiance responsivity calibration is

$$R_{\text{DUT}} = \frac{i_{\text{DUT}}}{i_{\text{trap}}} R_{\text{trap}} = \frac{i_{\text{DUT}}}{i_{\text{trap}}} s_{\text{trap}} A, \quad (1)$$

where R_{DUT} is the irradiance responsivity of the device under test, R_{trap} is the irradiance responsivity of the trap, s_{trap} is the power spectral responsivity of the trap, A is the area of the aperture on the trap, and i is the photocurrent. The photocurrent is converted to voltage in a transimpedance amplifier and then measured with a multimeter.

Equation (1) assumes that the reference planes of the DUT and trap are in the same plane, i.e., that the defining apertures are located the same distance from the point source. In many cases, they are located in different planes. In Subsection 2.D.4, it is shown that, for the aperture sizes and operating distances used on SIRCUS, the sources can be treated as point sources. For a point-source geometry,

$$I(\lambda) = E_1(\lambda)d_1^2 = E_2(\lambda)d_2^2, \quad (2)$$

where $I(\lambda)$ is the radiant intensity of the source; E_1 is the irradiance at reference plane 1, located a distance d_1 from the source; and E_2 is the irradiance at reference plane 2, located a distance d_2 from the source. In many cases, the reference plane of the DUT is not known and must be determined radiometrically.

There are two types of uncertainty components, designated Type A and Type B. Type A uncertainties are evaluated using statistical methods, and Type B uncertainties are evaluated using models or other external information. The term standard uncertainty refers to an estimated standard deviation. Assuming each uncertainty component is independent from the others (the components are uncorrelated), the combined standard uncertainty is the root sum square of the individual uncertainty components. Often, the different variables are not completely independent from one another, and correlations between these variables need to be taken into account.^{34,35}

The expanded uncertainty is the product of the combined standard uncertainty and a coverage factor k , where the value of k is chosen based on the desired level of confidence. Typically the expanded uncertainty is reported with $k = 2$, corresponding to a confidence level of 95%. A confidence level of 95% means that there is a 1 in 20 chance that a measurement will fall outside the interval. A coverage factor $k = 3$ corresponds to a confidence level of 99%, meaning there is a 1% chance that a measurement will fall outside the stated interval. In reporting the uncertainty for a measurement, the components of standard uncertainty are listed and their designation stated (A or B). The uncertainty table should also identify and distinguish random components from systematic components that are common to all wavelengths. This information is important when combining the spectral measurements, for example in measuring the band-integrated response of filtered detectors.

The dominant uncertainties of the spectral irradiance responsivity scale originate from systematic errors in the absolute scale transfer from the cryogenic radiometer. Temperature variations within the facil-

Table 1. SIRCUS Uncertainty for an Irradiance Responsivity Calibration

Uncertainty Component	Relative Standard Uncertainty [%]	
	Type A	Type B
Reference detector responsivity		
Radiant power responsivity (400 to 920 nm)	0.025	
Aperture area	0.004	
Response uniformity	0.005	
Cosine dependence	0.01	
Polarization		0.00
Linearity	0.00	
Temperature		0.003
Source characteristics		
Radiant flux	0.005	
Wavelength (<0.01 nm)		0.005
Irradiance uniformity	0.005	
Determination of the reference plane	0.01	
I-V Gain	0.01	
Voltmeter reading		0.005
Irradiance		0.032
Transfer to device under test (estimated)		0.030
Combined standard uncertainty ($k = 1$) (%)		0.044

ity, while small, may also contribute to the overall uncertainty in certain spectral regions. The radiometric stability of the source (and monitor detector) and the irradiance uniformity at a reference plane contribute to the overall uncertainty in the measurement. Additional uncertainties from the radiometric characteristics of the DUT need to be quantified to establish the uncertainty in the calibration (and subsequent measurements of a source). Typically, the instrument's response linearity, temperature dependence, polarization dependence, and out-of-FOV blocking are measured. The current-to-voltage converter and the multimeter used to measure the signal need to be characterized and their contribution to the overall uncertainty established. Finally, both short-term stability (repeatability) and long-term stability (to monitor degradation in time) should be considered.

In the following subsections, we discuss the uncertainty components in a typical irradiance responsivity calibration. The components are combined into an uncertainty budget in Table 1. These are representative numbers only. The uncertainty in an irradiance responsivity calibration may differ slightly, depending on the details of the calibration and the DUT.

1. Detector-Based Spectral Irradiance Responsivity Scale

The reference standard tunnel-trap detectors hold the spectral irradiance responsivity scale on SIRCUS. As no light is reflected back from the trap detector to the aperture, the aperture area and the trap detector spectral radiant power responsivity can be determined sep-

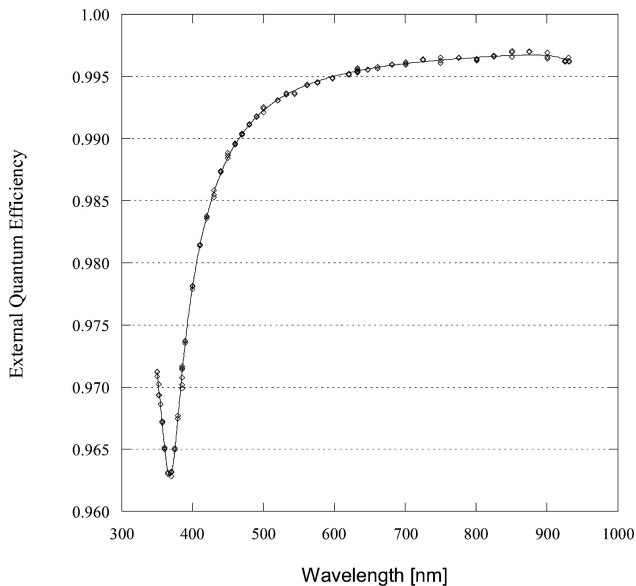


Fig. 4. Silicon tunnel-trap detector EQE versus wavelength.

arately. The spectral irradiance responsivity of the trap detector is calculated as the product of the aperture area and the spectral radiant power responsivity of the trap detector. The spectral radiant power responsivity of the tunnel trap was measured by direct substitution against the working standard ACR (Section 2). The spectral power responsivity (in A/W) is proportional to the EQE and the wavelength. The proportionality factor is e/hc , where e is the elementary electron charge, c is the speed of light in vacuum, and h is the Planck constant. The measured EQE of one of the working standard trap detectors (T-01) versus the wavelength (82 laser wavelengths) is shown in Fig. 4. The EQE is equal to 0.996 to within 0.1% between 600 and 920 nm. The relative combined standard uncertainties in the detector responsivity are 0.05% between 400 and 960 nm and 0.1% between 350 and 400 nm. A fit to the data points, illustrated in Fig. 4, shows that the reproducibility error of the responsivity determinations is very small, especially between 500 and 900 nm. That is, the uncertainty in the fit to the EQE is smaller than the uncertainty determination at each wavelength. Additionally, there are correlations among these absolute points.³⁵ Neither have been considered or included in the uncertainty budget listed in Table 1.

The trap detector was then equipped with a precision circular aperture whose area was measured on an interferometrically controlled x - y translation stage with a video microscope by using edge detection.²⁵ The relative standard uncertainty of the area determination for the 5 mm diameter aperture of the trap detector was 0.004%.²⁵

The spectral radiant power responsivity of the reference standard trap detectors was measured in underfilled (total beam power measurement) mode. In the irradiance mode, the incident flux overfills the aperture. The radiant flux falls on different regions of the trap detector for the two measurement modes. While

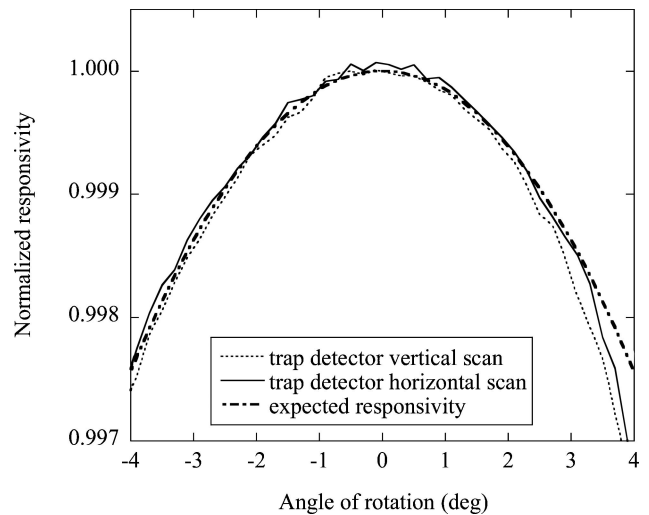


Fig. 5. Angular responsivity of the tunnel-trap detector.

typically small for silicon trap detectors, the spatial nonuniformity in responsivity of the trap detector can produce the ultimate limiting uncertainty component for the reference irradiance responsivity scale when the primary standard, in our case the ACR, measures radiant power. Dust is the primary cause of nonuniformity in the responsivity because the reference trap detectors are nonwindowed devices. To propagate the low uncertainties in power responsivity to irradiance responsivity, the detector's spatial response uniformity, as well as the area of the defining aperture, must be measured. The response of a reference trap detector was recently found to be uniform to within 0.01% over the entire area of the entrance window (with the aperture removed).

When measuring a point source, the expected responsivity in irradiance mode is a cosine dependence on the angle of rotation of the detector from the plane normal to the incident flux. Deviations from the expected response can give rise to errors when measuring extended sources. Figure 5 shows the normalized angular responsivity of the tunnel-trap detector when it is equipped with a circular aperture of 5 mm in diameter. The responsivity deviation from the cosine function is less than 0.02% within a 6° FOV. For an 8° FOV, the deviation is approximately 0.05%. This feature makes it possible to use these trap detectors as transfer standards for monochromator-based facilities where the beam convergence angle is smaller than the unvignetted FOV of the tunnel-trap detector.

2. Radiometric Characteristics of the Trap Detector. The radiation from an integrating sphere is typically unpolarized.³⁶ If polarized light is required for a calibration, a collimator can be used with a polarizer in the beam.

Linearity is easily checked by changing the laser power with the intensity stabilizer at the input to the fiber. The ratio of the signal of the DUT or reference trap to the monitor signal as a function of power should

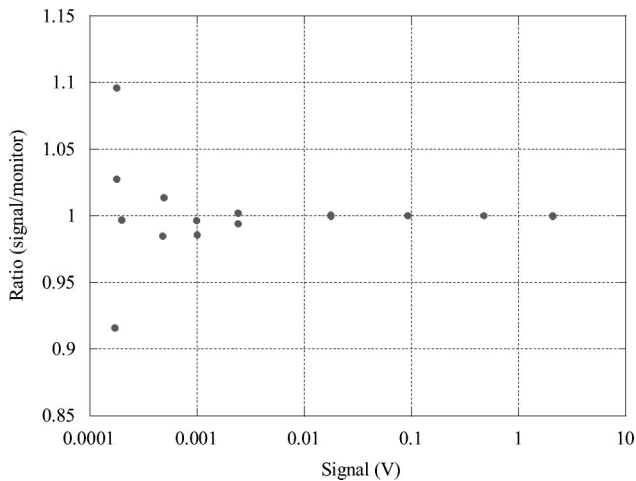


Fig. 6. Detector response linearity. The signal-to-monitor ratio as a function of the signal (related to incident optical power).

be a straight horizontal line. Figure 6 is a representative plot of a silicon detector's response linearity over four decades. Some silicon detectors have been measured to be linear over 14 decades.^{37,38}

The temperature in the SIRCUS facility was maintained at a nominal temperature of 22 °C. Typical variations were of the order of 0.5 °C or less, though in extreme cases, variations of the order of ± 2 °C were observed. The temperature, pressure, and humidity inside the light-tight enclosure can be monitored and corrections can be made if necessary. The temperature coefficient of Hamamatsu S1337 photodiodes (the type of silicon photodiode used in the trap detectors) has been measured.¹ It was found that there was negligible dependence below 950 nm ($<0.01\%/K$) but that the dependence rose quickly to $\sim 0.2\%/K$ by 1000 nm.³⁹ A similar dependence should be seen in trap detectors using these diodes.

3. Source Characteristics

The radiant power and wavelength stability are two of the primary uncertainty components. A laser intensity stabilizer keeps the laser power level constant to within 0.1%. The lasers used as excitation sources are equipped with etalons to reduce the wavelength uncertainty from mode hopping. The wavelength uncertainty is of the order of 10^{-3} nm with a typical bandwidth of the order of 10^{-3} nm. The wavelength uncertainty is dominated by the dependence of the index of refraction of air on temperature, humidity, and pressure. The wavemeter corrects for the temperature and pressure dependence and can be programmed to correct for the humidity.

The sequence for measurements of a DUT is to first measure the trap and monitor signal, then move the stage so that the DUT versus the monitor signal is measured, then move back to the trap measurement. If any change is observed in the trap-to-monitor ratio greater than $\sim 0.01\%$, additional measurements are made and the data are averaged. Typically, from 9 to 16 samples are averaged for each data point. Occa-

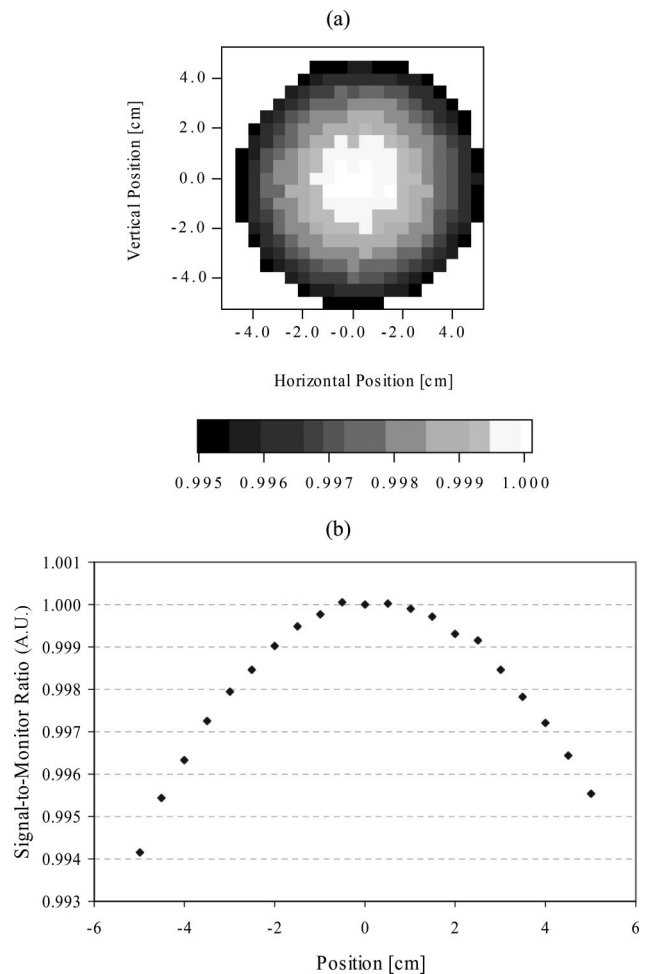


Fig. 7. Irradiance uniformity at a reference plane 1 m from the irradiance source. (a) Two-dimensional map of the irradiance distribution; (b) horizontal slice through the vertically centered irradiance.

sionally additional samples are taken, for example, when measuring the out-of-band response of a filter radiometer under test.

The irradiance at a reference plane should be spatially uniform to limit the magnitude of corrections for different size entrance pupils. In Fig. 7(a) we show the irradiance distribution at a reference plane approximately 1 m from the exit port of a 25.4 mm integrating sphere equipped with a 5 mm diameter aperture. In Fig. 7(b) we show a horizontal slice across the center of the distribution. As shown in Fig. 7, the irradiance is uniform to within 0.1% over the central ± 2 cm in both the horizontal and vertical directions. The entrance apertures of most irradiance meters calibrated on SIRCUS have diameters significantly smaller than 4 cm, and no correction for irradiance nonuniformity at the reference plane is applied.

4. Distance

The distance between the source and trap detector apertures (reference planes) is measured optically and mechanically. For a point-source geometry, the irradiance should follow an inverse square law, i.e., the ir-

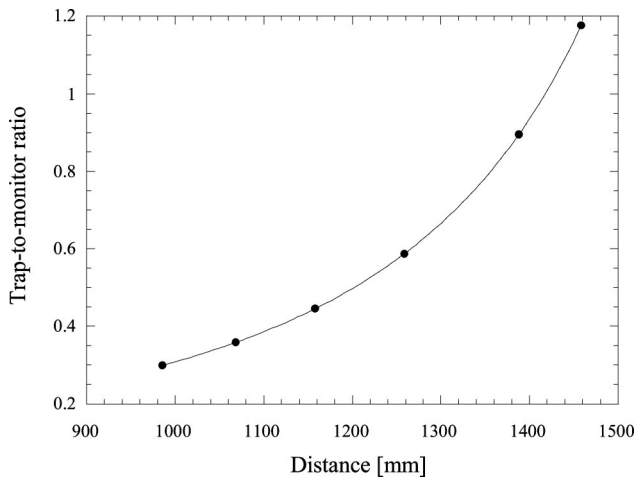


Fig. 8. Radiometric determination of the distance between two aperture planes. Dots are measured trap-to-monitor ratios; solid curve is a fit to the data.

radiance should be a function of $1/d^2$, where d is the distance between the two reference planes. The relative distance between the source and the detector is measured with an electronic ruler that has a quoted resolution of $5\ \mu\text{m}$.⁴⁰ The three-axis detector translation stage is moved in the horizontal direction, and the detector and monitor signals are acquired as a function of relative distance. The ratio of the trap signal to the monitor signal is then plotted as a function of distance and fit with a nonlinear least-squares algorithm.⁴¹ Figure 8 illustrates an optical distance measurement, with the dots measuring trap-to-monitor ratios and the solid curve being the fit to the data. The data were fit to the expression

$$y = m_1 / (m_0 - m_2)^2, \quad (3)$$

where the radiant intensity is given by m_1 , the zero offset of the fixed source is m_2 , and m_0 is the position of the stage measured by the electronic ruler. The uncertainty in the fit to m_2 is $28.7\ \mu\text{m}$. Since we know the zero offset from this fit, we also know the absolute separation at any value of the electronic ruler with an uncertainty of $28.7\ \mu\text{m}$. To validate the radiometric measurements, we also measured the aperture separation by using a calibrated ruler. The two separate techniques used to measure the distance between the source and the detector reference planes agreed usually within $50\ \mu\text{m}$. Given a $50\ \mu\text{m}$ uncertainty in the trap reference plane, the uncertainty in the irradiance at a given reference plane for distances of 1 m or greater is less than 0.01%.

For radiometers with a known reference plane, we use a micrometer to make sure that the DUTs and the reference trap aperture lie in the same plane. By using a micrometer, the reference planes can be aligned to within approximately $10\ \mu\text{m}$. Consequently, this approach significantly reduces the uncertainty in the irradiance at the DUT reference plane. If the DUT reference plane is not known, it is optically determined by using Eq. (3). For a non-point-source geometry, the full equation including the spatial extent of

the source and detector is required⁴²; the uncertainties remain the same.

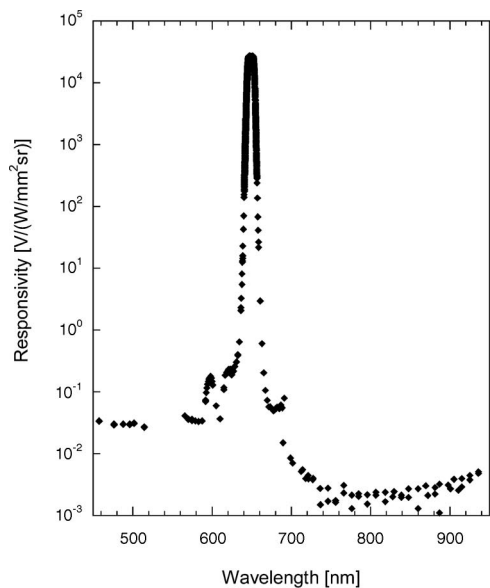
5. Current-to-Voltage Conversion (I - V Amplification)

The uncertainty of the current-to-voltage (I - V) conversion⁴³ was 0.01% for gain selections between $10^4\ \text{V/A}$ and $10^7\ \text{V/A}$. At these gains, the uncertainty of the feedback resistors in the I - V converter was 0.01% ($k = 1$) for the decade nominal resistance values. The uncertainty increased to 0.014% at the $10^8\ \text{V/A}$ gain where two $50\ \text{M}\Omega$ resistors (each with 0.01% resistance uncertainty) were connected serially. Because the resistance uncertainty of $10^9\ \Omega$ resistors is 0.5% or higher, a gain of $10^9\ \text{V/A}$ was radiometrically calibrated against a gain of $10^8\ \text{V/A}$ by measuring the same stabilized optical power. The gain uncertainty for this highest gain selection was 0.02%. The low uncertainties in gain can be achieved only if the dark reading is subtracted from the signal plus the dark reading of the trap detector radiometer (which includes the I - V converter) using a shutter positioned upstream in the laser beam. The temperature coefficients of the resistances were $0.001\%/^\circ\text{C}$ for gain selections between $10^4\ \text{V/A}$ and $10^7\ \text{V/A}$. The maximum temperature change in the light-tight box is $2\ ^\circ\text{C}$. Given an equal probability distribution for the temperature, the uncertainty in the resistance arising from the temperature coefficient is $(0.001\%) \times 2/3 = 7 \times 10^{-4}\%$.³³

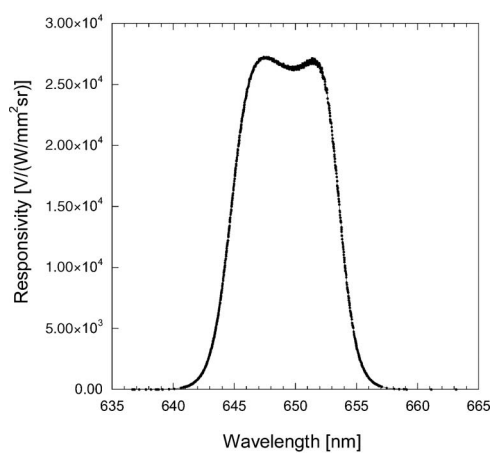
6. Transfer to Test Instrument

To achieve the lowest possible uncertainties on SIRCUS, the instrument should be designed with the calibration in mind. The uncertainty in the transfer to a test instrument is listed in Table 1 as 0.03%. This is for a well-designed, well-characterized, stable radiometer. Nonideal instrument characteristics such as stability, temperature dependence, long-term drift, and out-of-field response, all contribute to increased overall uncertainty in a calibration. Interference fringes from multiple reflections of incident radiation at optical surfaces have been observed in the calibration of instruments with windows and other optical elements if they are not wedged or antireflection coated. For example, the absolute spectral responsivity of a pyrometer (discussed in Subsection 4.A) calibrated on SIRCUS is shown in Fig. 9, in both a logarithmic [Fig. 9(a)] and a linear [Fig. 9(b)] scale. Interference fringes (the sinusoidal oscillations in the responsivity) are emphasized in the expanded view [Fig. 9(c)]. The presence of interference fringes increases the difficulty in the calibration if they must be measured during the calibration or increases the uncertainty in the calibration.

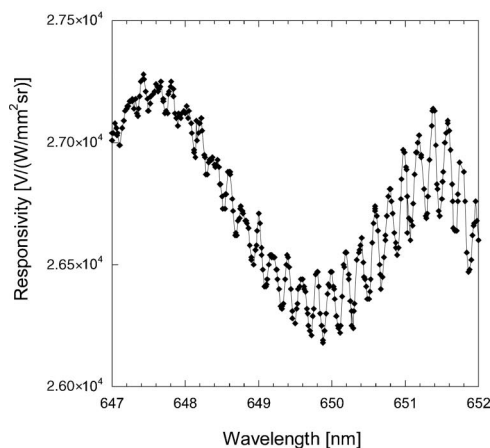
As an aside, we have found that interference fringes are ubiquitous, caused mainly by the window on the photodiode or parallel-surface windows in the device, or filters.¹² A complete mapping of the fringes is possible on SIRCUS because of the narrow spectral bandwidth and wavelength stability of the lasers and because the laser wavelength can be tuned automatically. In certain calibration approaches—for example,



(a)



(b)



(c)

Fig. 9. Absolute spectral irradiance responsivity of a filter radiometer, namely, the AP1 pyrometer, shown on (a) a logarithmic and (b) a linear scale. (c) Expanded view of the responsivity showing large oscillations arising from multiple reflections of the incident flux between surfaces within the instrument.

using lamp-monochromator systems—the fringes are not observed. Interference fringes occur when the coherence length of the source is as long as or longer than the size of the interfering structure. For example, interference fringes will most likely be present from multilayer coatings even for an incoherent source such as a lamp. If they are not observed, it is likely because the fine structure in the spectral responsivity caused by interference fringes is being averaged over the finite source bandwidth. However, the averaging may not be complete, and artifacts caused by the incomplete cancellation of the fringes can lead to erroneous results. Also, errors can arise in the determination of an instrument's effective aperture area using the scanning method if fringes are present.¹² In this case, the instrument should be calibrated directly in the irradiance mode to obtain the lowest achievable uncertainties.

7. Radiance Responsivity Calibrations

For radiance responsivity calibrations, the uncertainty budget differs only slightly from the uncertainty budget derived for irradiance responsivity calibrations. In a radiance responsivity calibration, the average radiance over the entire integrating sphere exit port area is measured by the reference trap detector, while instruments being calibrated typically image variously sized central regions of the exit port. Errors in calibration can occur if the sphere radiance is nonuniform, giving different average radiance depending on the area of the exit port being imaged. While the sphere's nonuniformity can be mapped and corrections applied, for the lowest uncertainty measurements, it is desirable to keep the sphere's nonuniformity as small as possible. Many researchers have calculated baffle arrangements for spheres to improve the radiance uniformity within the exit port for different input source configurations. We have found empirically that if the input laser beam impinges on the sphere wall close to the exit port, no baffles inside the sphere are needed.

The integrating spheres used for radiance responsivity calibrations on SIRCUS have been designed to allow the incident laser light to hit the sphere wall near the exit port. The spatial uniformity of one of the spheres, a 30 cm diameter Spectralon-coated integrating sphere with a 7.5 cm diameter aperture, was mapped using a radiometer with a narrow ($\sim 1^\circ$) FOV. Fixed at a distance of 0.5 m from the sphere, the target spot diameter of the radiometer at the sphere exit port was approximately 12.5 mm. The radiometer was translated in 6 mm increments and the radiance recorded at each position. The sphere radiance was spatially uniform to within $\pm 0.1\%$ over the entire sphere exit port (Fig. 10). Radiance is a conserved quantity. As long as the DUT is imaging an area within the exit port, the distance from the DUT to the sphere exit port is not critical for radiance responsivity calibrations.

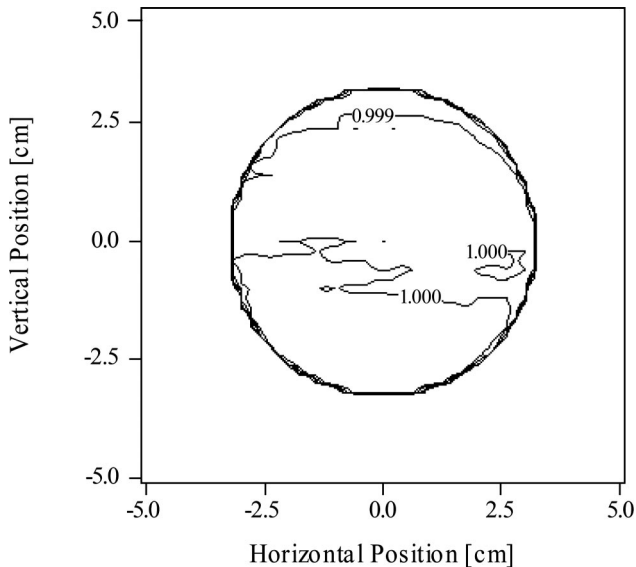


Fig. 10. Contour plot of the sphere radiance uniformity within the exit port; 0.1% steps.

E. Calibration Procedure

Before an instrument can be calibrated, it must be aligned with respect to the integrating sphere, as must the reference standard detector. To align the system, a laser is used to define an optical axis. Both the integrating sphere and the detectors are then aligned to the optical axis. The optical axis is typically set to be parallel to the direction of motion of a linear translation stage that moves perpendicular to the sphere exit port (the z axis defined in Fig. 11). The z axis translation stage sits on a pair of rails and is manually translated. A linear encoder records the stage position along the rails.

As illustrated in Fig. 11, to define the optical axis, a laser beam is incident on a pellicle beam splitter that is mounted on the z -axis rail system. A mirror is positioned behind the pellicle to retroreflect the light directly back into the laser. The pellicle is in a mirror mount and is adjusted to reflect light that is then aligned to be parallel to the translation stage. This is done by first mounting an iris near the pellicle beam splitter on the translation stage and

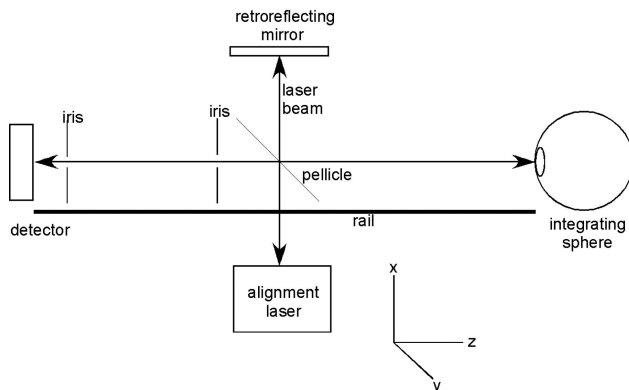


Fig. 11. Schematic of the alignment method for SIRCUS.

aligning it so that the laser light is centered on the iris aperture. Then the iris is moved by using the translation stage to lie some distance away from the pellicle. The angle of the pellicle beam splitter is adjusted so that the light reflected from it goes through the iris aperture. These two steps are repeated until the beam is centered on the iris at the two translation stage positions. At this point, the optical beam is parallel to the translation stage, and the optical axis is defined.

To align the detectors, the motorized x - y translation stage is positioned such that the laser is centered on each detector (one at a time), and the reflection from a flat reference plane on the detector is parallel with the incident beam. For each detector, a computer registers and stores the alignment position. The retroreflected beam (from the mirror behind the pellicle) is automatically aligned parallel to the rail. The sphere exit port is then centered on this beam (and the angle adjusted to coalign the reflected laser beam with the incident beam).

The alignment between the detectors and the integrating sphere is radiometrically validated by translating the detectors in the x and y directions and recording the signals as a function of stage position. The stage position giving the maximum signal from each instrument is compared with the stage position derived from the optical alignment procedure. The two positions typically agree to within 1 mm, well within the desired alignment uncertainty.

1. Calibration Protocol

The entire data collection sequence is automated. Initially, an electronic shutter that blocks the laser radiation before it enters the optical fiber is closed, and a background signal is acquired for both the reference standard trap detector and the sphere monitor. Then the shutter opens and the signals from the trap and the monitor on the sphere are recorded. The signals are initially amplified using a current-to-voltage amplifier⁴⁴ and then fed into a digital multimeter.⁴⁵ The signal from the multimeter is averaged for several seconds. The mean reference-to-monitor ratio and the standard deviation of the ratio are recorded. After this, the stage moves to the DUT position, and the data acquisition sequence is repeated. This gives the DUT mean signal-to-monitor ratio and the standard deviation of the ratio. The standard deviations of the ratios are monitored; trap detector measurement standard deviations larger than 0.01% are an indication of laser power instabilities.

Under routine calibration conditions, the intensity-stabilized laser wavelength is read by the wavemeter and transferred to the computer during each measurement. Along with mean ratios, the mean and standard deviations of the wavelength are recorded. This allows ready identification of laser wavelength instabilities during a scan. Occasionally, for faster data acquisition, the wavelength is recorded only at the beginning of the acquisition sequence. Following the data acquisition

sequence, the wavelength is changed and the sequence is repeated.

3. Comparison with the National Institute of Standards and Technology Lamp–Monochromator-Based Calibration Facility

The high optical power available with laser-based calibration systems enables us to calibrate instruments directly for either radiance or irradiance responsivity. The low wavelength uncertainty of the laser is instrumental in reducing the calibration uncertainty for filtered instruments. The source radiance uniformity also permits rapid characterization and calibration of digital imaging systems. Some of the advantages of the laser-based calibration approach over a conventional lamp–monochromator-based approach are illustrated by the calibration of a photoelectric pyrometer (PEP), an instrument used to radiometrically determine the temperature of a blackbody.⁴⁶ The instrument is equipped with a narrow bandpass filter (~1 nm) for spectral selectivity.

For accurate radiance temperature determinations, the instrument’s spectral out-of-band responsivity must be measured as well as its in-band responsivity. Figure 12 shows the relative spectral responsivity of

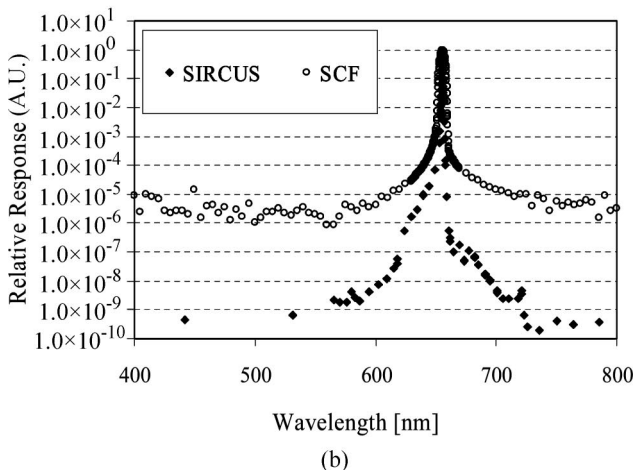
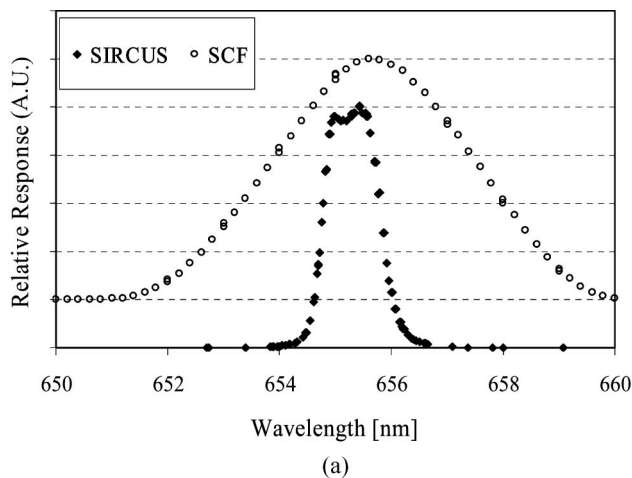


Fig. 12. Relative spectral responsivity of the PEP measured on SIRCUS and on the SCF: (a) linear scale; (b) log scale.

the PEP determined on SIRCUS compared with the relative spectral responsivity determined using the lamp–monochromator system in the SCF. As shown in Fig. 12(a), the spectral responsivity measured with the lamp–monochromator system is dominated by the spectral bandwidth of the source and deconvolution of the spectrum by using the source slit scatter function is required. In contrast, the fine detail in the spectral responsivity is easily measured on SIRCUS because of the monochromatic nature of the source. Note that there are several overlying data points at each wavelength along both the rising and falling edges, demonstrating the extreme wavelength stability of the SIRCUS facility. Because of the low flux in the lamp–monochromator system, the out-of-band responsivity is limited to approximately 10^{-6} [Fig. 12(b)]. In contrast, the out-of-band responsivity can be measured to the 10^{-9} level in the SIRCUS facility.

In SIRCUS, instruments are calibrated in their operational state: at the system level, with entrance pupils overfilled. This approach avoids unforeseen errors that can occur using other calibration approaches. For example, consider the measurements of the relative spectral responsivity of a single channel filter radiometer known as a standard lamp monitor (SLM).⁴⁷ The SLM can be operated in irradiance or radiance mode, depending on the foreoptics. The irradiance mode configuration has a Teflon diffuser, a window, an interference filter, and a silicon photodiode. The instrument’s relative spectral responsivities (RSRs) are used to band integrate the response to an illumination source. The RSR of a SLM was measured on the SCF. During these measurements, the flux from the monochromator exit slit was imaged onto the center of the diffuser. In this case, the irradiance collector was underfilled by the incident radiant flux. The SLM was also calibrated in irradiance mode for absolute spectral responsivity on SIRCUS. In this case, the irradiance collector was overfilled by the flux from the laser-illuminated integrating sphere. A comparison of the two results by using peak-normalized data showed that the relative spectral responses did not agree (Fig. 13). There was no dependence on the $f/\#$ of the incoming flux. However, spatial maps of the relative response at multiple

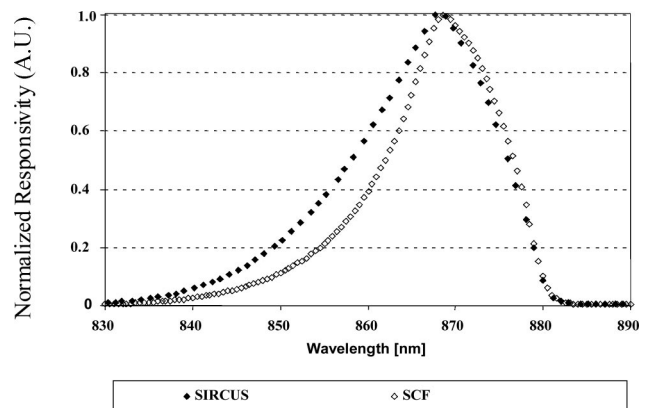


Fig. 13. Relative spectral responsivity of the SLM measured in underfilled mode (SCF) and in overfilled mode (SIRCUS).

fixed wavelengths within the in-band region showed that the irradiance responsivity was not spatially uniform (due to the diffuser), leading to the observed differences. These measured differences can cause errors in the band-averaged measurements of spectral irradiance when the spectrum of the source being measured differs from that of the calibration source.

4. Application to Primary Radiometric Quantities and Units

The NIST Optical Technology Division is responsible for maintaining two fundamental SI units, the unit for temperature, the kelvin, above 1234.96 K, and the unit for luminous intensity, the candela. In the following subsections we describe the effect of SIRCUS calibrations on reference standard pyrometers used to measure the radiance temperature of blackbody sources and photometers used to measure the illuminance of standard lamps. Using SIRCUS to develop a detector-based validation of the spatial distribution of the radiant flux from a standard synchrotron source predicted by the Schwinger equation is also discussed.

A. Radiance Temperature

For temperatures above the freezing temperature of silver, the ITS-90 (Ref. 48) is defined in terms of spectral radiance ratios to one of the silver-, gold-, or aluminum-freezing temperature blackbodies using the Planck radiance law.⁴⁹ In the ITS-90, the assigned temperatures for the aluminum, silver, and gold freezing points result from thermometry using ratio pyrometry from the mean of two different and conflicting constant-volume gas thermometry measurements at lower temperatures. There are thermodynamic temperature uncertainties of the freezing points of the primary metal blackbodies that arise primarily from the uncertainties in the lower temperature gas thermometry.

Because of the use of spectral radiance ratios, the temperature uncertainties of ITS-90 assigned blackbody, $u(T_{\text{BB}})$, increase as the square of the temperature ratios according to

$$u(T_{\text{BB}}) = \frac{u(T_{\text{FP}})}{T_{\text{FP}}^2} T_{\text{BB}}^2, \quad (4)$$

where T_{FP} and $u(T_{\text{FP}})$ are the temperature and the uncertainty of the fixed-point blackbody and T_{BB} is the temperature of the higher temperature blackbody. The increases in the temperature uncertainties can be reduced by using absolute radiometry with pyrometers traceable to cryogenic radiometers, and the resulting temperature uncertainties can be smaller than those measured using the ITS-90 techniques.^{10,50}

To decrease the uncertainties in the radiance temperature scale at NIST and, ultimately, in the thermodynamic temperature assignment of the metal freezing-point temperatures, a pyrometer—denoted the Absolute Pyrometer-1 (AP1)—was built to radiometrically measure blackbody temperatures.^{50,51} Spec-

tral selection is achieved by using a narrowband interference filter with a center wavelength at 650 nm and a bandpass of 10 nm. The filter is temperature stabilized to near room temperature, and the hermetically sealed silicon photodiode has a two-stage thermoelectric cooler for operation at -15 °C. It has a noise-equivalent power (NEP) of 3 fW at an electrical bandwidth of 0.3 Hz. The radiometric characteristics, e.g., stability and linearity, for example, of the AP1 have been established.⁵¹

The AP1 was calibrated for absolute spectral radiance responsivity on SIRCUS. As shown in Fig. 9, it has a peak responsivity between 647 and 652 nm, a FWHM bandwidth of approximately 10 nm, and out-of-band blocking better than 10^{-7} . Interference fringes with an amplitude of 0.5% were observed in the responsivity. The absolute spectral responsivity was therefore measured with 0.03 nm resolution. The AP1 subsequently measured the melt and freeze cycles of silver and gold fixed-point blackbodies. The signal from the AP1 is converted to temperature using the equation:

$$i_u = \int s_L(\lambda) \varepsilon_u L_u(\lambda, T) d\lambda, \quad (5)$$

where $s_L(\lambda)$ is the absolute spectral responsivity of the AP1, ε_u is the emissivity of the blackbody, and $L_u(\lambda, T)$ is the radiance of the blackbody derived from Planck's equation.⁵⁰

The noise-equivalent temperature at the gold (and silver) freezing temperature is ≈ 2 mK, and the noise will not be the dominant component of the total temperature uncertainties. The AP1 was calibrated twice on SIRCUS, once in 2003 and again in 2005. Using the SIRCUS 2003 calibration, the expanded uncertainty ($k = 2$) in the radiometric measurement of the gold (or silver) freezing-point blackbody was approximately 0.15%. The radiometric uncertainties can be related to the uncertainties of the temperature determinations from the derivative of the Wien approximation, which shows the relationship between the uncertainty in radiance, L , to the uncertainty in blackbody temperature, T :

$$\frac{\Delta L}{L} = \frac{c_2 \Delta T}{\lambda T^2}. \quad (6)$$

In Eq. (6), c_2 is the second radiation constant, and λ is the wavelength. Using Eq. (6), an uncertainty of 0.15% in radiance responsivity at 650 nm will lead to an uncertainty of 121 mK in the measurement of the melting and freezing temperature of the gold-point blackbody, which is slightly larger than the ITS-90 uncertainty, as shown in Table 2.⁵² The AP1 was recently recalibrated on SIRCUS by using the 2004 trap-detector responsivity scale (Table 1). By using the new calibration, the expanded uncertainty in the radiometric measurement of the gold point is reduced to approximately 0.09%. With the reduced uncer-

Table 2. Comparison of the Results of Radiometric Determinations of the Gold- and Silver-Point Blackbody Temperatures Using the AP1 Pyrometer with the ITS-90 Values

	T_{AP1} (K)	$u(T_{AP1})$ (K) ($k = 2$)	T_{90} (K)	$u(T_{90})$ (K) ($k = 2$)	$T_{AP1} - T_{90}$ (K)
Au-point blackbody	1337.344	0.121	1337.33	0.100	0.014
Ag-point blackbody	1234.956	0.106	1234.93	0.080	0.026

tainty from SIRCUS, the corresponding temperature uncertainty derived from the uncertainty in the radiometric measurement of the gold-point blackbody can be reduced to approximately 72 mK, significantly lower than the ITS-90 uncertainty.

These results are, in effect, the first step toward implementation of a detector-based thermodynamic temperature scale. SIRCUS can be used to calibrate optical pyrometers directly, eliminating the dependence on a blackbody and the ITS-90. As discussed by Yoon *et al.*,^{50,53} moving from a source-based to a detector-based spectral irradiance (and radiance) scale can greatly reduce the radiometric uncertainty in the measurement of higher temperature sources.

B. Photometry

The redefinition of the candela in 1979 coupled photometric and radiometric units⁵⁴ and made it possible to realize and maintain photometric units by using detectors as well as sources. Following the redefinition, many national laboratories, including NIST, derived and maintained the candela (and derived photometric units) using calibrated standard detectors traceable to cryogenic radiometry rather than standard lamps traceable to primary standard blackbodies and international temperature scales.^{55,56} Since 1992, the candela has been maintained at NIST by using a group of eight standard photometers.⁵⁷ The overall relative expanded uncertainty ($k = 2$) for the NIST illuminance unit realization is currently 0.39%.⁵⁷

There are several components in the uncertainty budget related to the determination of the photometer relative spectral responsivity using the lamp-monochromator system in the SCF.^{1,57} The uncertainties in these components can be significantly reduced or eliminated by realizing the illuminance scale on SIRCUS. The spectral responsivity scale will be reduced from a standard uncertainty of 0.11% currently measured on the SCF to 0.075% because of the reduction of transfer steps from the high-accuracy cryogenic radiometer. The luminous efficiency function defined by the Commission Internationale de l'Éclairage (CIE), $V(\lambda)$, is a strong function of wavelength. The SIRCUS wavelength scale, with uncertainties reduced to less than 0.01 nm from the SCF's wavelength uncertainty of 0.1 nm, reduces the relative standard uncertainty for this component from 0.04% to <0.004%. A significant set of uncertainty components results from the geometry of the SCF

output beam. The SCF uses $f/9$ optics to focus the light to a 1 mm spot that is used to calibrate the photometers, whereas the photometers are normally used in a far-field condition. SIRCUS can calibrate photometers in a geometrical configuration identical to the application geometry, eliminating errors caused by different interreflection patterns inside the photometer between the calibration and application.

In addition, since SIRCUS calibrates the detector in irradiance mode instead of power mode, the uncertainty of the aperture size and the uncertainty due to the nonuniform spatial response of the photometer are eliminated. Combined the uncertainty contribution from these components can be reduced from 0.12% (Ref. 57) to less than 0.01%. The overall relative expanded uncertainty ($k = 2$) for the NIST illuminance unit realization is expected to be reduced to 0.24%, a 40% reduction from the uncertainty in the current scale, when the new illuminance scale is realized. The new illuminance scale will lead to an expected overall relative expanded uncertainty of 0.27% ($k = 2$) for the NIST candela.

The current photometric working standard photometers were not calibrated on SIRCUS because large interference fringes (of the order of 10%) were observed in the spectral responsivity of those instruments. A trap-detector-based tristimulus colorimeter was developed to realize a detector-based color scale (see Subsection 5.A.). As a first step toward the new SIRCUS-based photometric scale, the irradiance responsivity of the photometric (Y) channel of the colorimeter was determined. An aperture mounted on the front surface of the colorimeter defines the reference plane for irradiance and illuminance measurements. Because of the thick color filter combinations⁵⁸ and the removed photodiode windows, all four channels of this colorimeter showed fringe-free operation on SIRCUS. Use of feedback resistors in the photocurrent meters with 0.001%/°C temperature coefficient of resistance, 0.01% uncertainty of their decade nominal values, and realizing loop gains larger than 10^4 in dc measurements for all signal-gain selections, the uncertainty of the photocurrent-to-voltage conversion was 0.01%.³¹

From the SIRCUS-measured spectral irradiance responsivity of the photometric channel (between 360 and 950 nm), the illuminance responsivity was calculated.⁵⁹ Thereafter standard lamps were measured in the photometry calibration facility to compare the illuminance responsivities of the same channel determined from both the existing (SCF-based) and the new (SIRCUS-based) scales. The colorimeter was calibrated on SIRCUS twice, with the calibrations separated in time by 15 months. The illuminance responsivity of the photometric channel from the two SIRCUS calibrations agreed within 0.1%. The average illuminance responsivity from the two SIRCUS calibrations was 4.911 nA/lx, 0.35% higher than the SCF-based illuminance responsivity.

Our investigations showed that the SCF-based illuminance responsivity (used in the present photo-

metric scale) is low by approximately 3% because of a beam-clipping problem caused by the small apertures in the working standard photometers. Comparisons of the spectral responsivity determined on SIRCUS and the SCF show spectral shifts as large as 0.5 nm and responsivity differences as large as 1%.

C. Synchrotron Radiation

Schwinger described the nature of radiation that is emitted from the acceleration of relativistic particles.⁶⁰ In a synchrotron accelerator, electrons are confined to a circular path and continuously emit radiation tangential to their direction. Magnets are used to control the energy and direction of electrons in the synchrotron. Like blackbody radiation, synchrotron radiation is absolutely calculable from the knowledge of a very few parameters. Blackbody radiation follows from Planck's law: Knowledge of the temperature and emittance allows for calculation of all radiation emanating from the blackbody. Synchro-

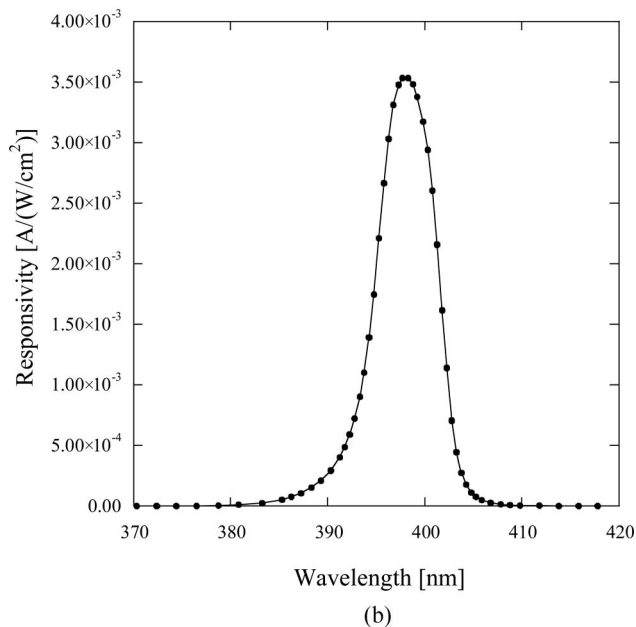
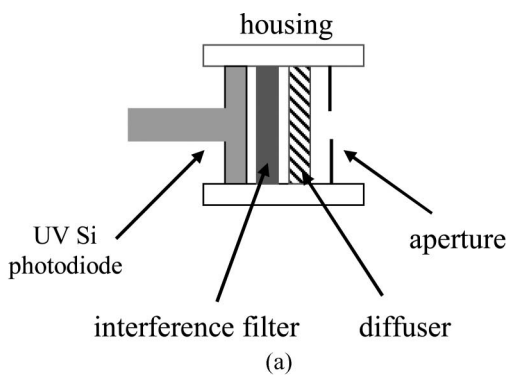


Fig. 14. (a) Schematic diagram of the filter radiometers that were calibrated for irradiance responsivity on SIRCUS and used to measure the angular distribution of radiation and intensity at SURF III. (b) Absolute spectral irradiance responsivity of the 400 nm filter radiometer.

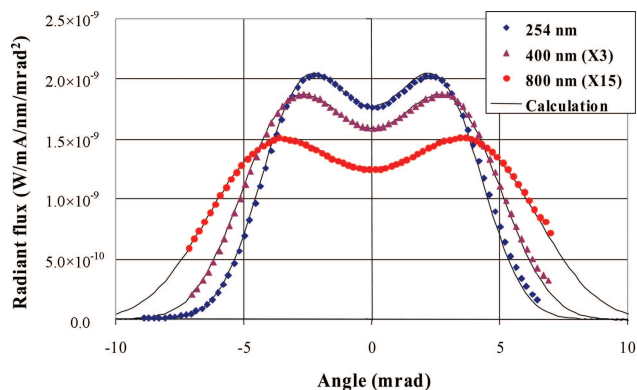


Fig. 15. (Color online) Angular distribution pattern from SURF measured with three filter radiometers. The solid curve is the calculated distribution pattern.

tron radiation is defined by the Schwinger equation: The electron beam current, magnetic field, and the orbital radius completely define the radiation field.

The NIST Synchrotron Ultraviolet Radiation Facility (SURF III) is a particularly simple synchrotron storage ring. The electrons are confined to a circular orbit in a vacuum chamber by a dipole magnet with an extremely uniform magnetic field ($<10^{-4}$ nonuniformity in the magnetic field). The angular distribution and intensity of radiation is dependent on the electron beam energy and the wavelength of the emitted radiation. To validate the expected spatial distribution, three filter radiometers were constructed with band-center wavelengths at 254, 400, and 800 nm, respectively. A simplified schematic of the filter radiometers is shown in Fig. 14(a). These filter radiometers contain a precision aperture, a diffuser, an interference filter, and a photodiode, and they are not polarization sensitive. The filter radiometers were calibrated for irradiance responsivity on SIRCUS; the absolute spectral responsivity of the 400 nm filter radiometer is shown in Fig. 14(b). They subsequently measured the angular distribution and intensity of the emitted radiation at a known beam current and magnetic field at SURF III.⁶¹ The filter radiometer results are shown in Fig. 15. By numerically integrating the response of the radiometers and the calculated angular distribution of the intensity of emitted radiation, the spatial distribution of the radiant flux from SURF III can be calculated for different wavelengths. The quantitative results for the three filter radiometer wavelengths are given by the solid curves in Fig. 15. There are no adjustable parameters in the calculations. The results at 400 nm have been multiplied by a factor of 3 and the results at 800 nm by a factor of 15 to show all the results on the same figure. The calculated, or predicted signals as a function of angle agree with the measurements to better than 0.5%.

5. Applications

The unique characteristics of SIRCUS give us the versatility to address a wide range of optical metrology issues in addition to applications related to the

measurement of fundamental sources or to the realization of fundamental SI units. We briefly discuss other applications in the following subsections.

A. Detector-Based Color Scale

A tristimulus colorimeter standard was developed by using temperature-stabilized filters in front of a silicon tunnel-trap detector to realize a detector-based color scale.⁵⁸ The tristimulus colorimeter is composed of four channels consisting of filter combinations with the trap detector designed to mimic the CIE color-matching functions⁶² with small spectral mismatch. The spectral mismatch of the realized channels is characterized by the CIE f_1' values.⁶³ The filter combinations are mounted in a temperature-controlled (heated) filter wheel that can be moved between the trap detector and the front aperture. The aperture plane is the reference plane of the illuminance-mode photometer-colorimeter, and it is in the plane of the front cover. A precision current-to-voltage converter is attached to the top of the instrument. Electronic and radiometric characterizations, including current-to-voltage conversion uncertainty and spatial, angular, and spectral responsivity, have been done.

The tristimulus colorimeter was calibrated on SIRCUS as a first step in the establishment of a detector-based color scale.⁶⁴ When utilizing the uniform irradiance at the detector reference plane from the small sphere source of the SIRCUS, the nonuniformity of spatial responsivity of the filters and the detector in the tristimulus colorimeter will not contribute to measurement uncertainty. Also, interreflections between optical components will be the same for the calibration and subsequent applications, and their contribution to radiometric measurement error will cancel. The combined expanded uncertainties ($k = 2$) in the absolute spectral irradiance responsivities of the individual channels, neglecting correlations, are estimated to be 0.15% or less. From the spectral irradiance responsivity curves, the broadband calibration factors of the colorimeter channels can be calculated, and the tristimulus values of a test light source can be measured. For a Planckian radiator (a light source with a well-known spectral distribution), a 0.15% uncertainty in the spectral irradiance responsivity of any one channel of a tristimulus colorimeter will result in a chromaticity coordinate uncertainty of 0.0004 for both x and y . These uncertainties correspond to an uncertainty of 4 K in color temperature, a factor of 2 less than the uncertainties of current primary color temperature lamp standards.

B. Stray Light Characterization of Spectrographs

Spectrographs are spectroradiometers with multielement array detectors that can acquire an entire spectral image over some finite spectral region simultaneously. Spectrographs commonly consist of an entrance port, a dispersing element (such as a grating) to spatially resolve the spectral components of the incident radiation, and mirrors to image the entrance port (often a slit) onto a reference plane where the array detector is located. Because

of the dispersing element, the spatial image of the entrance port falls on different regions of the detector array, depending on its wavelength; broadband sources form an image across the entire array. The spectral coverage of a spectrograph is determined by the size of its detector array, the dispersion properties of its grating, and its optical layout. Compared with conventional, scanned grating systems, source spectral distributions can be acquired in a matter of seconds, as opposed to minutes. The ability to rapidly acquire a spectrum has led to the use of array-based systems in a variety of radiometric, photometric, and colorimetric applications where acquisition speed is an issue, for instance, on a production line, or in cases where the source being measured is not stable over extended periods of time.

The measurement uncertainties of spectrographs are often larger than conventional scanning spectrometers. Spectrographs are single grating instruments and there are intrinsic limitations in the background signal originating from radiation scattered from imperfections in the grating and other optical elements. This unwanted background radiation, called stray light, while small—of the order of 10^{-4} or less of the incident spectral radiance in a single grating spectrograph—can give rise to unforeseen errors, often much larger than anticipated, when the spectral distribution of a source being measured differs significantly from the spectral distribution of the calibration source. In comparison, a conventional scanning spectrometer is often constructed as a double-monochromator instrument (double grating or prism grating) that has a stray light level lower than 10^{-6} .

In many applications, the spectral distributions of the test source and the calibration source differ significantly. Spectrometers are typically calibrated against standard incandescent lamps with correlated color temperatures (CCTs) ranging from 2800 to 3100 K. Most of the emission from these sources lies in the red and NIR regions. Measurement errors, often significant, arising from stray light are inevitable when instruments calibrated against standard lamps subsequently measure light sources that have dissimilar spectral distributions, such as LEDs, displays, discharge lamps, and fluorescent lamps. In these situations, stray light is often the dominant source of spectrograph measurement error.

Algorithms have been developed to correct the output of a spectrograph for stray light based on the spectral imaging properties of the instrument. The tunable lasers available on SIRCUS are used to characterize a spectrograph's response for stray light. Figure 16 is a semilogarithm plot of spectra acquired from a spectrograph with excitation wavelengths ranging from 350 to 800 nm. Each spectrum is a single image normalized by the peak value. The strong central peak in each image (or spectrum) in Fig. 16 corresponds to the image of the entrance slit formed on the detector array. The broad shoulder and finite baseline are signals from radiation that is not

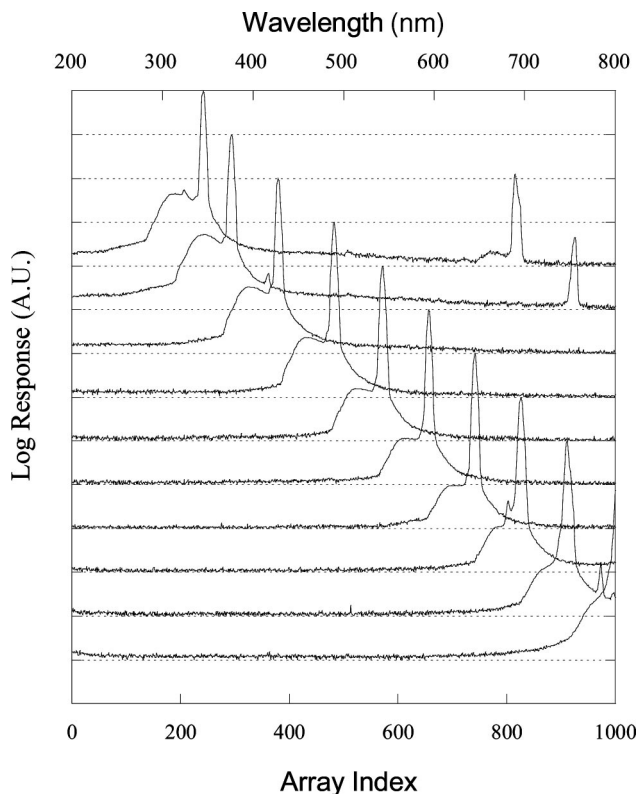


Fig. 16. Spectrograph images as the incident wavelength is changed and the central image moves across the array.

properly imaged onto the detector, i.e., from stray light within the spectrograph. By measuring the system response at a number of wavelengths, the evolution of the image as the excitation wavelength moves across the array can be determined. Based on these measurements, a stray light correction algorithm can be implemented that reduces the errors and associated uncertainties arising from stray light an order of magnitude or more.^{47,65,66} For an accurate characterization of spectrometers for this correction, the input optics must be illuminated by uniform monochromatic radiation at many wavelengths in irradiance or radiance mode. The SIRCUS facility is effectively utilized to achieve the necessary measurements.

C. Solar Irradiance

Sun photometers are filter radiometers used to determine atmospheric optical properties at different wavelengths. Primary standard reference sun photometers are calibrated at high altitudes by using the Langley–Bouguer technique. In this calibration approach, a series of measurements at different solar zenith angles are made over the course of a day, giving a range of measured signals as a function of zenith angle (or air mass). The measurements are then extrapolated back to zero air mass, giving an instrument signal corresponding to the expected signal in the absence of any intervening atmosphere.⁶⁷ Reductions in the uncertainties in irradiance responsivity calibrations of primary standard reference Sun photometers using laboratory standards would allow for meaningful com-

parisons with the results from the Langley–Bouguer method, resulting in independent values for the exoatmospheric solar irradiance at the set of measurement wavelengths.

Global networks of Sun photometers are used to provide detailed mapping of atmosphere optical properties, for example, aerosol concentrations and distributions. Sun photometers that are part of the Aerosol Robotic Network⁶⁸ (AERONET) are calibrated for irradiance responsivity against reference primary standard Sun photometers using the cross-calibration technique at the NASA Goddard Space Flight Center (GSFC).⁶⁷ The cross-calibration technique consists of near-simultaneous solar observations with the uncalibrated instrument and a calibrated reference Sun photometer. Reducing the uncertainties in network instruments by using laboratory standards would validate the uncertainties in the calibration transfer and could improve the characterization of the atmosphere.

Because Sun photometers measure solar irradiance, their responsivity is typically low, and they are difficult to calibrate using lamp–monochromator systems. To demonstrate the feasibility of calibrating Sun photometers on SIRCUS, two multichannel Sun photometers were calibrated and the results compared with standard cross calibrations.⁶⁹ To compare the cross-calibration results to the SIRCUS calibrations, the SIRCUS-derived irradiance responsivities $s(\lambda)$ were used to predict a top-of-the-atmosphere (TOA) signal $V_o(\text{SIRCUS})$:

$$V_o(\text{SIRCUS}) = \int s(\lambda)E(\lambda)d\lambda, \quad (7)$$

where $s(\lambda)$ is the spectral responsivity of one of the radiometer channels and $E(\lambda)$ is an exoatmospheric solar irradiance spectrum. In this work we used the exoatmospheric solar irradiance spectrum developed by Thuillier *et al.*⁷⁰ To perform the integration, the $s(\lambda)$ and the $E(\lambda)$ were interpolated to a uniform wavelength interval of 0.25 nm and integrated. The 750 nm channel results agreed with the cross calibration to within 0.15%, the 490 nm channel to within 0.85%, and the 440 nm channel to within 5.76%.

The dominant source of uncertainty in the SIRCUS-based predicted TOA signal was the uncertainty in the solar irradiance spectrum. Assuming an $\sim 1.5\%$ combined standard uncertainty in the absolute value and given a step size of 1 nm in the region of interest, we were able to validate the cross calibration with an expanded uncertainty ($k = 2$) of $\sim 4\%$. The agreement for the 490 and 750 nm channels were within the combined uncertainties, but the 440 nm results were not and warrant further investigation.

The measurements demonstrated that SIRCUS irradiance levels were high enough to calibrate Sun photometers. Current uncertainties in the exoatmospheric solar irradiance depend on the wavelength, but in atmospheric transmittance windows in the vis-

ible spectral region, they are estimated to be approximately 0.5% to 1%. Calibration of primary standard Sun photometers on SIRCUS with 0.1% uncertainties or less would enable us to differentiate between exoatmospheric solar irradiance spectra and could lead to a reduction in the uncertainties in the exoatmospheric solar irradiance spectrum. This has implications for global climate change studies because the exoatmospheric solar irradiance is one of the primary forcing functions driving the global climate.

Additional applications include the development of wavelength standard reference materials with reduced uncertainty⁷¹ and the characterization and calibration of instruments with large entrance pupils, such as telescopes and remote-sensing sensors.⁷²

6. Summary

We have described a laser-based calibration facility for irradiance- and radiance-measuring instruments. In this facility, high-power tunable lasers were introduced into integrating spheres by using optical fibers, producing uniform, quasi-Lambertian, highly radiant flux sources. Reference standard irradiance detectors, calibrated directly against national primary standards for spectral power responsivity, were used to determine the irradiance at a reference plane. Instruments were calibrated directly in irradiance or radiance mode with uncertainties approaching or lower than those available for spectral power responsivity calibrations in traditional lamp-monochromator facilities. The implications for fundamental radiometric measurements, including radiance temperature, photometric, and synchrotron source measurements, were described. Finally, advanced applications to realize the first detector-based color scale, to correct stray light in spectrographs, and to measure solar irradiance by using this facility were briefly outlined.

Work continues on reducing the uncertainties associated with measurements on SIRCUS as well as the spectral coverage and laser powers available. In Table 1 we calculated the uncertainty in the irradiance responsivity at a single wavelength. In practice, in determining the uncertainty in measuring the irradiance of a source by using a filter radiometer as an example, the responsivity was integrated over a wavelength range. The irradiance responsivity was determined for a large number of wavelengths, typically 100 or more, over the in-band range. Calculating the band-integrated responsivity, the random components in the uncertainty budget were reduced by the square root of the number of measurements, and only systematic components in the uncertainty budget contributed to the uncertainty in the measurement. We have neglected the reduction in the uncertainty from integrating the responsivity over a finite number of elements.

The spectral coverage of the SIRCUS facility for spectral responsivity calibrations is determined by the high-reflectance range of the coating of the integrating sphere sources, the wavelength coverage of the standard reference and monitor detectors, and the spectral coverage of the tunable laser systems. Spectralon and similar PTFE-based coatings have

high reflectance from 250 to 2500 nm. The spectral coverage of the UV-Vis-NIR SIRCUS facility has been extended into the UV and the short-wave infrared (SWIR) regions with the integration of a quasi-continuous-wave, mode-locked OPO-sum-frequency system. This system gave us nearly continuous tunability from 210 to 3.0 μm .

Research is being conducted on reference detectors to extend the radiant power responsivity scale from 350 down to 200 nm and from 1 out to 2.5 μm and beyond. Reference UV reflectance-type trap detectors using nitride-passivated UVG-100 diodes⁷³ as well as PIN-UV100 diodes⁷³ have been developed to extend the wavelength coverage from 350 down to 200 nm. Recently, a UV trap detector was calibrated for radiant power responsivity over the spectral range from 210 to 400 nm with an expanded uncertainty ($k = 2$) of 0.05% or less. Finally, a variety of irradiance-measuring working standard radiometers have been developed for the NIR range, including single-element Ge, InGaAs, and extended InGaAs detectors.^{74,75} With their calibration against an ACR, the low uncertainty in the SIRCUS irradiance scale will be extended into the IR spectral range.

The authors thank the U.S. Air Force Metrology for funding this work under contract 98-435. They also acknowledge the early and continued support of John Grangaard, USAF (ret.) and the significant contributions to the work by B. Carol Johnson, Howard Yoon, Yuqin Zong, Thomas C. Larason, C. Cameron Miller, and Ping-Shine Shaw from the NIST Optical Technology Division.

References

1. T. C. Larason, S. S. Bruce, and A. C. Parr, *Spectroradiometric Detector Measurements* (U.S. Government Printing Office, 1998).
2. T. R. Gentile, J. M. Houston, J. E. Hardis, C. L. Cromer, and A. C. Parr, "National Institute of Standards and Technology high-accuracy cryogenic radiometer," *Appl. Opt.* **35**, 1056–1068 (1996).
3. T. R. Gentile, J. M. Houston, and C. L. Cromer, "Realization of a scale of absolute spectral response using the NIST high-accuracy cryogenic radiometer," *Appl. Opt.* **35**, 4392–4403 (1996).
4. G. Eppeldauer, M. Racz, and T. Larason, "Optical characterization of diffuser-input standard irradiance meters," in *Proc. SPIE* **3573**, 220–224 (1998).
5. O. G. Peterson, S. A. Tuccio, and B. B. Snavelly, "cw operation of an organic dye solution laser," *Appl. Phys. Lett.* **17**, 245–247 (1970).
6. J. M. Yarborough, "cw dye laser emission spanning the visible spectrum," *Appl. Phys. Lett.* **24**, 629–630 (1974).
7. A. R. Schaefer and K. L. Eckerle, "Spectrophotometric tests using a dye-laser-based radiometric characterization facility," *Appl. Opt.* **23**, 250–256 (1984).
8. A. R. Schaefer, R. D. Saunders, and L. R. Hughey, "Intercomparison between independent irradiance scales based on silicon photodiodes physics, gold-point blackbody radiation, and synchrotron radiation," *Opt. Eng.* **25**, 892–896 (1986).
9. K. D. Mielenz, R. D. Saunders, and J. B. Shumaker, "Spectroradiometric determination of the freezing temperature of gold," *J. Res. Natl. Inst. Stand. Technol.* **95**, 49–67 (1990).
10. N. P. Fox, J. E. Martin, and D. H. Nettleton, "Absolute spectral

- radiometric determination of the thermodynamic temperatures of the melting/freezing points of gold, silver, and aluminum,” *Metrologia* **28**, 357–374 (1991).
11. V. E. Anderson, N. P. Fox, and D. H. Nettleton, “Highly stable, monochromatic and tunable optical radiation source and its application to high accuracy spectrophotometry,” *Appl. Opt.* **31**, 536–545 (1992).
 12. M. Noorma, P. Toivanen, F. Manoocheri, and E. Ikonen, “Characterization of filter radiometers with a wavelength-tunable laser source,” *Metrologia* **40**, S220–S223 (2003).
 13. A. Sperling, Physikalisch-Technische Bundesanstalt, Braunschweig, Germany (personal communication, 2005).
 14. J. M. Houston and J. P. Rice, “NIST reference cryogenic radiometer designed for versatile performance,” *Metrologia* **43**, S31–S35 (2006).
 15. L-1 Standards and Technology, Ijamsville, Md.
 16. D. J. Pugh and K. Jackson, “Automatic gauge block measurement using multiple wavelength interferometry,” in *Proc. SPIE* **656**, 244–250 (1986).
 17. T. F. Johnston, R. H. Brady, and W. Proffitt, “Powerful single-frequency ring dye laser spanning the visible spectrum,” *Appl. Opt.* **21**, 2307–2316 (1982).
 18. T. F. Johnston, “Lasers, dye,” in *Encyclopedia of Physical Science and Technology*, R. A. Meyers, ed. (Academic, 2002), pp. 315–359.
 19. L. E. Jusinski and C. A. Taatjes, “Efficient and stable operation of an Ar⁺-pumped continuous-wave ring laser from 505–560 nm using a coumarin dye,” *Rev. Sci. Instrum.* **72**, 2837–2838 (2001).
 20. P. F. Moulton, “Spectroscopic and laser characteristics of Ti:Al₂O₃,” *J. Opt. Soc. Am. B* **3**, 125–133 (1986).
 21. Spectra-Physics, Inc., Wavetrain frequency doubler with a Coherent, Inc. Model 899 Ti:sapphire laser.
 22. W.-L. Zhou, Y. Mori, T. Sasaki, S. M. Nakai, K. Nakano, S. Niikura, and B. Craig, “Intracavity frequency doubling of a continuous wave Ti:sapphire laser with over 70% conversion efficiency,” *Appl. Phys. Lett.* **66**, 2463–2465 (1995).
 23. T. R. Gentile and C. L. Cromer, “Mode-locked lasers for high-accuracy radiometry,” *Metrologia* **32**, 585–587 (1996).
 24. W. S. Hartree, P. R. Haycocks, and N. P. Fox, “The use of a mode-locked laser for ultraviolet radiometry,” *Metrologia* **35**, 339–343 (1998).
 25. J. Fowler and M. Litorja, “Geometric area measurements of circular apertures for radiometry at NIST,” *Metrologia* **40**, S9–S12 (2003).
 26. Spectralon, Labsphere, Inc., No. Sutton, N.H.
 27. E. A. Early, B. C. Bush, S. W. Brown, D. W. Allen, and B. C. Johnson, “Radiometric calibration of the Scripps Earth Polychromatic Imaging Camera,” in *Proc. SPIE* **4483**, 77–84 (2001).
 28. T. Stone, U.S. Geological Survey, Flagstaff, Ariz., (personal communication, 2005).
 29. E. F. Zalewski and C. R. Duda, “Silicon photodiode device with 100% external quantum efficiency,” *Appl. Opt.* **22**, 2867–2873 (1983).
 30. Hamamatsu, “Photodiodes,” Catalog 1990-91, 16.
 31. G. P. Eppeldauer and D. C. Lynch, “Opto-mechanical and electronic design of a tunnel-trap Si- radiometer,” *J. Res. Natl. Inst. Stand. Technol.* **105**, 813–828 (2000).
 32. G. Eppeldauer, “Noise-optimized silicon radiometers,” *J. Res. Natl. Inst. Stand. Technol.* **105**, 209–219 (2000).
 33. *Guide to the Expression of Uncertainty in Measurement* (International Organization for Standardization, Geneva, 1993).
 34. J. L. Gardner, “Correlated color temperature-uncertainty and estimation,” *Metrologia* **37**, 381–384 (2000).
 35. J. L. Gardner, “Correlations in primary spectral standards,” *Metrologia* **40**, S167–S176 (2003).
 36. K. R. Lykke, P.-S. Shaw, L. M. Hanssen, and G. P. Eppeldauer, “Development of a monochromatic, uniform source facility for calibration of radiance and irradiance detectors from 0.2 micrometer to 12 micrometer,” *Metrologia* **35**, 479–484 (1998).
 37. G. Eppeldauer and J. E. Hardis, “Fourteen-decade photocurrent measurements with large-area silicon photodiodes at room temperature,” *Appl. Opt.* **30**, 3091–3099 (1991).
 38. G. Eppeldauer, M. Racz, and L. M. Hanssen, “Spectral responsivity determination of a transfer-standard pyroelectric radiometer,” in *Proc. SPIE* **4818**, 118–126 (2002).
 39. G. P. Eppeldauer, S. W. Brown, T. C. Larason, M. Racz, and K. R. Lykke, “Realization of a spectral radiance responsivity scale with a laser-based source and Si radiance meters,” *Metrologia* **37**, 531–534 (2000).
 40. Burgthaler Elektronik GmbH.
 41. KaleidaGraph, Synergy Software, Reading, Pa.
 42. J. H. Walker, R. D. Saunders, J. K. Jackson, and D. A. McSparron, *Spectral Irradiance Calibrations* (U.S. Government Printing Office, 1987).
 43. G. Eppeldauer, *Optical Radiation Measurement with Selected Detectors and Matched Electronic Circuits between 200 nm and 20 μm* (U.S. Government Printing Office, 2001).
 44. Stanford Research Systems model SR570 or home built.
 45. Hewlett Packard Model HP3458A.
 46. C. E. Gibson, B. K. Tsai, and A. C. Parr, *Radiance Temperature Calibrations* (U.S. Government Printing Office, 1998).
 47. S. W. Brown, D. K. Clark, B. C. Johnson, H. W. Yoon, K. R. Lykke, S. J. Flora, M. E. Feinholz, M. A. Yarbrough, R. A. Barnes, Y. S. Kim, T. Stone, and J. Mueller, eds., *Advances in Radiometry for Ocean Color* (NASA, 2004).
 48. H. Preston-Thomas, “The international temperature scale of 1990 (ITS-90),” *Metrologia* **27**, 3–10 (1990).
 49. D. Halliday and R. Resnick, *Fundamentals of Physics* (Wiley, 1981).
 50. H. W. Yoon, D. W. Allen, C. E. Gibson, R. D. Saunders, B. C. Johnson, S. W. Brown, and K. R. Lykke, “Temperature scales using radiation thermometers calibrated from absolute irradiance and radiance responsivity,” in *NCSL International Workshop and Symposium* (Orlando, Fla., 2003).
 51. D. W. Allen, R. D. Saunders, B. C. Johnson, C. E. Gibson, and H. W. Yoon, “The development and characterization of an absolute pyrometer calibrated for radiance responsivity,” in *International Temperature Symposium* (Chicago, Ill., 2003).
 52. H. W. Yoon, C. E. Gibson, D. W. Allen, R. D. Saunders, M. Litorja, S. W. Brown, G. P. Eppeldauer, and K. R. Lykke, “The realization and the dissemination of the detector-based kelvin,” in *Proceedings of Tempmeko 04* (Dubrovnik, Croatia, 2004).
 53. H. W. Yoon, C. E. Gibson, and P. Y. Barnes, “Realization of the National Institute of Standards and Technology detector-based spectral irradiance scale,” *Appl. Opt.* **41**, 5879–5890 (2002).
 54. *Principles Governing Photometry* (Bureau International des Poids et Mesures, 1983).
 55. R. L. Booker and D. A. McSparron, *Photometric Calibrations* (U.S. Government Printing Office, 1987).
 56. C. L. Cromer, G. Eppeldauer, J. E. Hardis, T. Larason, and A. C. Parr, “National Institute of Standards and Technology detector-based photometric scales,” *Appl. Opt.* **32**, 2936–2948 (1993).
 57. Y. Ohno, *NIST Measurement Services: Photometric Calibrations* (U.S. Government Printing Office, 1997).
 58. G. P. Eppeldauer and M. Racz, “Design and characterization of a photometer-colorimeter standard,” *Appl. Opt.* **43**, 2621–2631 (2004).
 59. G. P. Eppeldauer, S. W. Brown, C. C. Miller, and K. R. Lykke, “Improved accuracy photometric and tristimulus-color scales based on spectral irradiance responsivity,” *Proceedings of the*

25th Session of the Commission Internationale de l'Eclairage, Vol. 1, pp. D2-30–D32-33 (2003).

60. J. Schwinger, "On the classical radiation of accelerated electrons," *Phys. Rev.* **75**, 1912–1925 (1949).
61. P.-S. Shaw, U. Arp, H. W. Yoon, R. D. Saunders, A. C. Parr, and K. R. Lykke, "A SURF beamline for synchrotron source-based radiometry," *Metrologia* **40**, S124–S127 (2003).
62. R. McCluney, *Introduction to Radiometry and Photometry* (Artech House, 1994).
63. J. D. Schanda, "Colorimetry," in *Handbook of Applied Photometry*, C. DeCusatis, ed. (Springer, 1998), pp. 327–412.
64. G. P. Eppeldauer, "Spectral response based calibration method of tristimulus colorimeters," *J. Res. Natl. Inst. Stand. Technol.* **103**, 615–619 (1998).
65. S. W. Brown, B. C. Johnson, M. E. Feinholz, M. A. Yarborough, S. J. Flora, K. R. Lykke, and D. K. Clark, "Stray-light correction algorithm for spectrographs," *Metrologia* **40**, S81–S84 (2003).
66. Y. Zong, S. W. Brown, K. R. Lykke, and Y. Ohno, "A simple spectral stray light correction method for array spectroradiometers," *Appl. Opt.* **45**, 1111–1119 (2006).
67. C. Pietras, M. Miller, R. Frouin, E. J. Welton, and I. Slutsker, "Calibration of sun photometers and sky radiance sensors," in *In Situ Aerosol Optical Thickness Collected by the SIMBIOS Program (1997–2000): Protocols, Data QC, and Analysis*, R. B. G. S. Fargion and C. McClain, eds. (NASA Goddard Space Flight Center, 2001).
68. B. N. Holben, T. F. Eck, I. Slutsker, D. Tanre, J. P. Buis, A. Setzer, E. Vermote, J. A. Reagan, Y. J. Kaufman, T. Nakajima, F. Leaven, I. Jankowiak, and A. Smirnov, "Aeronet—a federated instrument network and data archive for aerosol characterization," *Remote Sens. Environ.* **66**, 1–16 (1998).
69. N. Souaidia, C. Pietras, G. Fargion, R. A. Barnes, R. Frouin, K. R. Lykke, B. C. Johnson, and S. W. Brown, "Comparison of laser-based and conventional calibrations of sun photometers," in *Proc. SPIE* **4481**, 61–72 (2003).
70. G. Thuillier, M. Herse, T. Foujots, W. Peetermans, W. Gillotay, P. C. Simon, and H. Mande, "The solar spectral irradiance from 200 to 2400 nm as measured by the SOLSPEC spectrometer from the ATLAS and EUREKA missions," *Sol. Phys.* **214**, 1–22 (2003).
71. E. A. Early, NIST, Gaithersburg, Md. (personal communication, 2005).
72. T. Stone, U.S. Geological Survey, Flagstaff, Ariz. (personal communication, 2005).
73. R. Korde, International Radiation Detectors, Inc., Torrance, Calif. (personal communication, 2005).
74. G. Eppeldauer, "Near infrared radiometer standards," in *Proc. SPIE* **2815**, 42–54 (1996).
75. G. Eppeldauer, "Electronic characteristics of Ge and InGaAs radiometers," in *Proc. SPIE* **3061-97**, 833–838 (1997).